





# DIPLOMARBEIT

# Optimal Power System Damping through Local Actuation

ausgeführt zum Zwecke der Erlangung des akademischen Grades eines Diplom-Ingenieurs unter der Leitung von

Univ.Prof. Dr. Stefan Jakubek Institut für Mechanik und Mechatronik Abteilung für Regelungstechnik und Prozessautomatisierung

eingereicht an der Technischen Universität Wien

Fakultät für Maschinenwesen und Betriebswissenschaften

von







# TU **Bibliothek**, Die approbierte gedruckte Originalversion dieser Diplomarbeit ist an der TU Wien Bibliothek verfügbar wern vour knowledge hub The approved original version of this thesis is available in print at TU Wien Bibliothek.

# Eidesstattliche Erklärung

Ich erkläre eidesstattlich, dass ich die Arbeit selbständig angefertigt, keine anderen als die angegebenen Hilfsmittel benutzt und alle aus ungedruckten Quellen, gedruckter Literatur oder aus dem Internet im Wortlaut oder im wesentlichen Inhalt übernommenen Formulierungen und Konzepte gemäß den Richtlinien wissenschaftlicher Arbeiten zitiert, durch Fußnoten gekennzeichnet bzw. mit genauer Quellenangabe kenntlich gemacht habe.

Wien, am 10. August 2025



Kurzfassung ii

# Kurzfassung

Für Wechselstrom-Versorgungsnetze stellen oszillierende Schwankungen in der Netzfrequenz eine erhebliche Bedrohung für den stabilen Betrieb dar. Die Dämpfung solcher Oszillationen und damit auch die Stabilität von solchen Stromnetzen beruht in hohem Maße auf großen mechanischen Trägheitsmomenten von Turbinen und Generatoren in lokal fokussierten Kraftwerken. Diese traditionellen Methoden der Netzfrequenzdämpfung werden allerdings zunehmend durch den wachsenden Anteil erneuerbarer Energieträger an ihre Grenzen gebracht. Allen voran sind hier die wachsenden Anteile von Wind- und Solarenergie zu erwähnen, die in verhältnismäßig vielen kleinen Anlagen mit geringem mechanischen Trägheitsmoment erzeugt werden.

In der vorliegenden Arbeit wollen wir diese Transformation zu erneuerbaren Energieträgern vereinfachen und die Stabilisierung von Versorgungsnetzen verbessern, indem wir kritische Oszillationen nur durch geschickte Aktuierung einer einzelnen Netzwerkkomponente dämpfen.

Um diesen Ansatz zu untersuchen, haben wir eine Simulationsumgebung aufgesetzt, die uns nicht nur erlaubt detaillierte Netzmodell zu simulieren, sondern auch Linearisierungen dieses Modells automatisch zu generieren. Mithilfe dieser Linearisierungen entwerfen wir aktive dämpfende Regler für die wichtigsten Oszillationsmodi des Kundur-2-Area System. Anhand dieser resultierenden Reglern zeigen wir, dass diese Oszillationen der Netzfrequenz durch den gezielten Eingriff einer einzelnen Netzwerkkomponente effektiv gedämpft werden können.

Die vorgestellten Regler bewerkstelligen diese Frequenzdämpfung basierend auf einiger weniger, sorgfältig ausgewählter Messgrößen von anderen Netzwerkkomponenten und wirken ausschließlich auf die Erregerspannung des lokalen Synchrongenerators. Dennoch wurde stets darauf geachtet, dass die verwendeten Entwurfsmethoden auch eine Anwendung auf Versorgungsnetzen mit Inverter-basierten Netzwerkkomponenten erlau-

Die erreichte Frequenzdämpfung soll die generellen Möglichkeiten lokaler Aktuierung aufzeigen und eine Referenz für weitere adaptive oder unabhängigere Ansätze darstellen.



Abstract iii

# Abstract

Frequency oscillations in power grids pose a notable threat to the stability of such systems. The damping of such oscillations and, with it, the operational stability of power grids, relies to a great extent on large mechanical inertia of turbines and generators of concentrated power plants. However, the growth of the share of renewable energy resources in power systems, in particular wind and solar power which introduce more distributed, low-inertia plants, challenges this traditional way of counteracting grid frequency oscillations.

In this thesis, we want to facilitate a further transformation towards larger shares of renewable energy resources and increase the stability of power systems by dampening hazardous frequency oscillations through clever actuation of just one single grid participant.

To examine our approach, we develop a simulation framework which allows an interconnected analysis of high-fidelity grid models and its linear representations. With this framework, we design active damping controllers for the most important frequency oscillation modes of the Kundur-2-Area System and show that the proposed controller, installed only in one single power plant, can drastically improve the oscillation behavior of the entire power grid.

The proposed controllers use only a few carefully selected feedback signals from other grid participants and achieve their damping performance by actuating only on the excitation voltage of a synchronous generator. However, the used controller design methods also allow their application on inverter-based power plants.

Therefore, the resulting damping performances demonstrate the general possibilities of local actuation and can be referenced as benchmarks for further more adaptive or independent approaches.



# Contents

1	Intr	oductio	on	1
2	Met	$\operatorname{hods}$		4
	2.1	Modeli	ng of Power Grids	4
		2.1.1	Synchronous Machine Model	8
		2.1.2	Additional Grid Components	11
		2.1.3	Simulink/Simscape Model of Power Grid	15
		2.1.4	Phasor Simulation	18
		2.1.5	Linearizing Simulink Models	19
		2.1.6	Handling feed-through Systems	21
		2.1.7	Loadstep Scenarios	23
	2.2	Contro	ollability and Observability of Modes	25
		2.2.1	Identification of Oscillation Modes	25
		2.2.2	Modal State Transformation	30
		2.2.3	PBH-Test	32
		2.2.4	Geometric Controllability and Observability	33
		2.2.5	Participation Factor	35
	2.3	Optima	al Controller Design	38
		2.3.1	Linear Quadratic Regulator	38
		2.3.2	Modal Weighting Matrix	40
		2.3.3	Linear Quadratic Regulator for Output Feedback	41
		2.3.4	Setpoint Tracking	44
3	Resi	ults		47
	3.1	Full St	ate Feedback	47
	3.2	Reduce	ed Set State Feedback	54
	3.3		ty Analysis	64
4	Con	clusion	and Outlook	68
$\mathbf{A}$	Desc	cription	n of state variables	70
Bi	bliog	raphy		72

# TU **Bibliothek**, Die approbierte gedruckte Originalversion dieser Diplomarbeit ist an der TU Wien Bibliothek verfügbar werk vourknowledge hub. The approved original version of this thesis is available in print at TU Wien Bibliothek.

List	of	Figu	ures
------	----	------	------

2.1	Full grid topology	5
2.2	Load units	6
2.3	Generator units	7
2.4	Steam Turbine Regulator and Model	13
2.5	Exciter Model	14
2.6	Power System Stabilizer Model	14
2.7	Loadstep simulation of reference system	26
2.8	Eigenvalues without controller	27
2.9		28
2.10		29
2.11	Controller block diagram	45
3.1	Eigenvalues with full-state-feedback controller	50
3.2	Results with full-state-feedback on Load 1 step	51
3.3	Results with full-state-feedback on Load 2 step	52
3.4	Power transfer with full-state-feedback	53
3.5	Eigenvalues with different controller configurations compared	55
3.6	Results with $\Delta \delta + \Delta \omega$ -feedback on Load 1 step	56
3.7	Results with $\Delta \delta + \Delta \omega$ -feedback on Load 1 step	57
3.8	Power transfer with $\Delta \delta + \Delta \omega$ -feedback	58
3.9	Results with $\Delta\omega$ -feedback on Load 1 step	59
3.10	Results with $\Delta\omega$ -feedback on Load 1 step	60
3.11		61
3.12	Eigenvalues from linearization series without controller	65
3.13	Eigenvalues from linearization series with $\Delta\delta + \Delta\omega$ -feedback controller .	66
3.14	Eigenvalues from linearization series with $\Delta\omega$ -feedback controller	67

# List of Tables

2.1	Synchronous Generator Model parameters	15
2.2	Steam Turbine and Regulator Model parameters	16
2.3	Exciter Model parameters	16
2.4	Power System Stabilizer Model parameters	17
2.5	Transformer Model parameters	17
2.6	Power Line Model parameters	17
2.7	Geometric controllability measures	34
2.8	Participation factors	37
3.1	Modal weights	49
3.2	Controller gains, part 1	62
3.3	Controller gains, part 2	63

# **TU Sibliothek**, Die approbierte gedruckte Originalversion dieser Diplomarbeit ist an der TU Wien Bibliothek verfügbar wien knowledge hub. The approved original version of this thesis is available in print at TU Wien Bibliothek.

# Chapter 1

# Introduction

Due to targets in CO2-emission reduction, as well as financial and strategic reasons, the share of energy in the European power system coming from renewable sources has continuously increased in recent decades. And due to the aforementioned reasons, this growth is projected to further continue. This evolution of the European power grid is largely driven by wind and solar power, which are the fastest growing energy resources [1]. The type of energy source is important because, compared to coal or nuclear power plants, wind and solar power introduce smaller and more distributed plants into the power system. However, traditional power grid frequency control relies a lot on the presence of large mechanical inertia of generator rotors from concentrated power plants [2, 3]. The large mechanical inertia provides energy storage in the form of kinetic energy and thus can compensate for gid imbalances after component faults or sudden changes in load demands. Additionally, power generators and consumers are not always synchronously coupled to each other via the same frequency of the alternating voltages. If the individual components are connected with power lines of considerable length, the power lines introduce a noticeable impedance to this coupling. This means the grid components are connected to each other with a certain degree of flexibility and thus are able to oscillate against one another. Large mechanical inertia also helps to keep those oscillation effects less critical and the concentration of power plants reduces the number of possible oscillation modes. Having said this, we have to consider that the grid frequency is one of the main indicators of the current power grid stability [4]. The focus on large power plants as main drivers of the grid frequency allowed manual tuning of asset control loops to stabilize oscillations within the grid frequency [5, 6]. Tuning of such stabilizing local control loops for power grids with much more distributed, low inertia grid participants, like wind and solar power plants, becomes, due to an increased number of parameters alone, already a much more difficult task though.

As the development of the power grid towards larger renewable energy shares has been an ongoing process for several decades, researchers came up with a wide variety of 1 Introduction 2

different approaches for improving grid stabilization. A lot of those approaches are still based on more traditional power grid structures with reasonably focused inertia in synchronous generators, whereas others elaborate the impact of low inertia grid forming power inverter control methods [7], or propose control algorithms which introduce a virtual inertia to the behavior of power inverters [8, 3, 9]. Some focus on algorithms to optimize parameters of multiple power grid components in a coordinated way, such as time constants and gains in [6] or virtual masses and damping factors in [2]. Others again introduce additional active grid components, for example flexible alternating-current transmission systems (FACTS-devices) with local feedback signals [10], or selectively add remote feedback signals to enhance the capabilities of conventional stabilization devices [11, 12]. The rotor speeds of different generators are also used as auxiliary feedback signals to further increase the effectiveness of additional active grid components like phase shifters [13] and power converters [14]. A comprehensive overview over similar inverter based approaches using wide-area measurement signals is given in [15]. Since the processing of such wide-area measurement signals heavily depends on a communication network for those signals, the authors in [16] even consider communication delays on additional inverter based grid components and in [17] put the scope of their work on the fault resistance of such approaches.

In this thesis however, we put a strong emphasis on generating an improvement in the frequency oscillation stability that can be achieved by just one single grid participant. Therefore we only integrate our proposed damping controllers into one single generator unit, whereas the rest of the power grid stays untouched. With this approach we facilitate the integration of damping controllers into existing grid infrastructure. We demonstrate that such a single local damping controller can successfully improve wide-area frequency oscillations. We showcase this on the Kundur-2-Area System, which is a renowned benchmark example for investigating frequency oscillation [5, 13, 11. Although we show the approach of a local stabilizing controller only for direct application on a synchronous generator, everything in this thesis was developed to allow a similar application on power converters.

Given this brief introduction to the dynamics of power grids, we provide a more detailed description of the Kundur-2-Area System simulation model and the methods to design optimal modal damping controllers for it in Chapter 2. In Section 2.1 we have an in-depth look at the working and implementation of all the components of the Kundur-2-Area System and how the complete power grid can be simulated in a MAT-LAB/Simulink framework. Furthermore we discuss how the MATLAB/Simulink framework not only lets us simulate a high-fidelity model of the power grid, but also lets us generate linearized representations in an automated way. Section 2.2 then contains the



1 Introduction 3

description of tools to identify specific oscillation modes and evaluate the controllability and observability of those modes. Finally in Section 2.3 we rewind the linear-quadraticregulatory method (LQR) to construct controllers for linear systems after an optimality principle. We then discuss how we can use the LQR method to construct controllers to purposefully dampen selected oscillating eigenvalues of the Kundur-2-Area System. Further, we also show how this can work not only for a full state feedback, but also if we only have a selected subset of the full state space available as feedback. In Chapter 3 we apply the proposed damping controllers on the Kundur-2-Area System and present their effect on the most hazardous oscillation modes. We compare controllers which are based on a full state feedback to controllers which are only based on a subset of states available as feedback signals. We showcase with the high-fidelity power grid simulation model that either of the proposed controllers have a remarkably good damping effect on the entire power grid, even though they are only installed in one single generator unit. This is then followed up by the conclusion in Chapter 4.



# Chapter 2

# Methods

# 2.1 Modeling of Power Grids

Throughout all analyses considered within this thesis the grid model topology is based on the original Kundur-2-Area System power grid model [5] and its corresponding MAT-LAB example implementation [18]. This grid topology can be considered a benchmark example for investigating oscillation effects between generators and is taken up in many other works on this topic [13, 11]. An overview of the grid topology is given in Fig. 2.1, where we can see the locations of the 4 generator unit and the loads as well as the lengths of the connecting power lines. More detailed illustration of the load and generator unit setups are given in Figs. 2.2 and 2.3 respectively. Its moderate number of modeled grid participants provides a good overview over the model, while still modeling multiple possible oscillation modes. Those possible oscillation modes can intuitively be recognized due to their different frequencies. For example the power lines between generator G1 and G2 are much shorter than the inter-area ones, resulting in a tighter connection of generator G1 to generator G2 compared to the connection of generator G1 to G3. Therefore we expect the oscillation between G1 and G2 (in-area-1) to have a higher eigenfrequency compared to the oscillation between G1 and G3 (inter-area). Consequently, the different oscillation modes also underlie varying degrees of controllability for specific system inputs. Intuitively, we expect the in-area-1 mode to be much more controllable from a control input at generator G1 than the in-area-2 mode, due to the closer location and tighter interconnection of the oscillation participants.

For simplicity of our grid model we will use symmetric power line lengths and parameters and identical synchronous generators. The generators are driven by identical steam turbines and accompanied by likewise identical exciter models.

The excitation systems of generator G2 and G3, as well as G1 only during all the reference/benchmark simulations, are additionally equipped with a so-called Power System Stabilizer (PSS) device. Those PSS devices use the generator shaft speed to improve

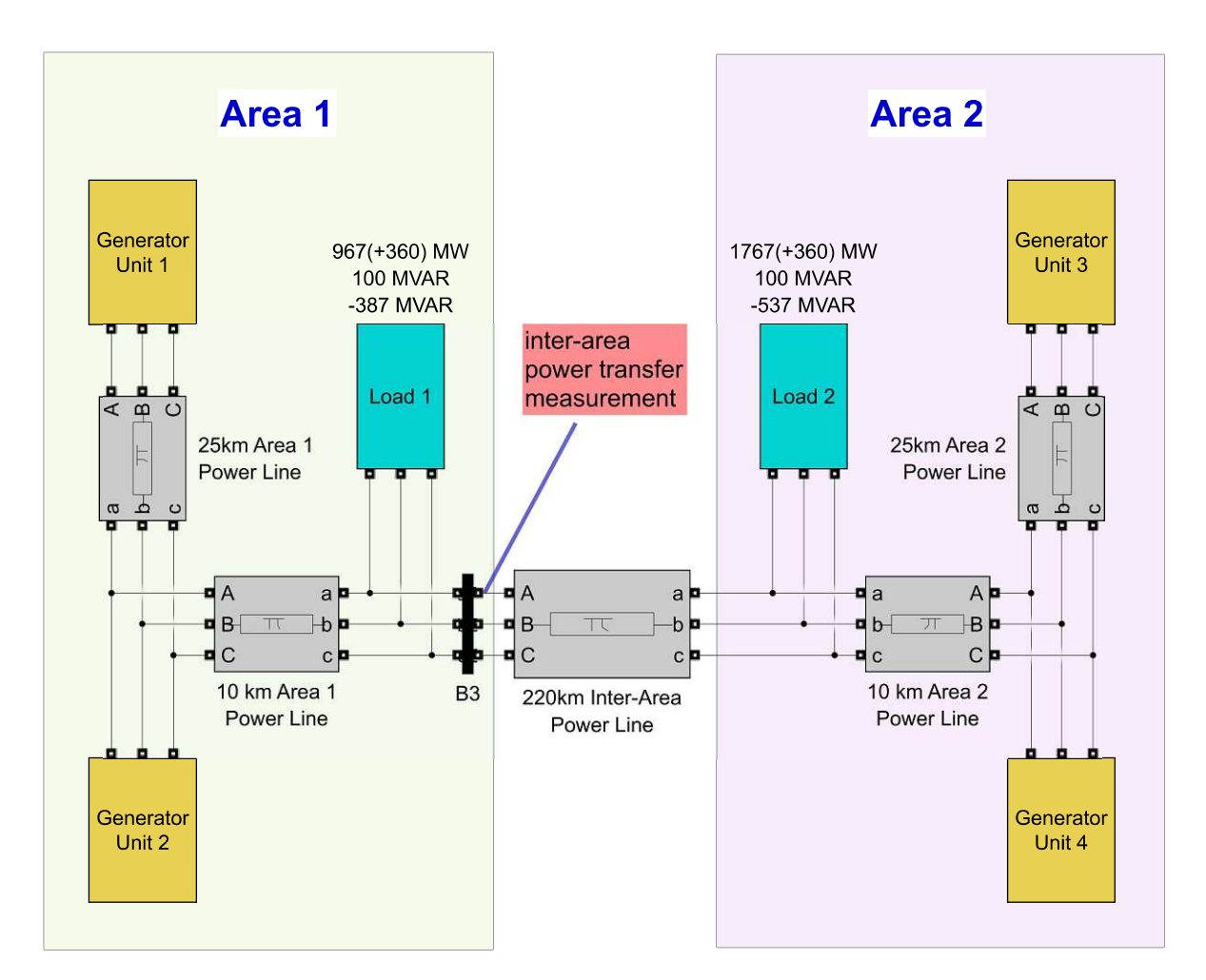
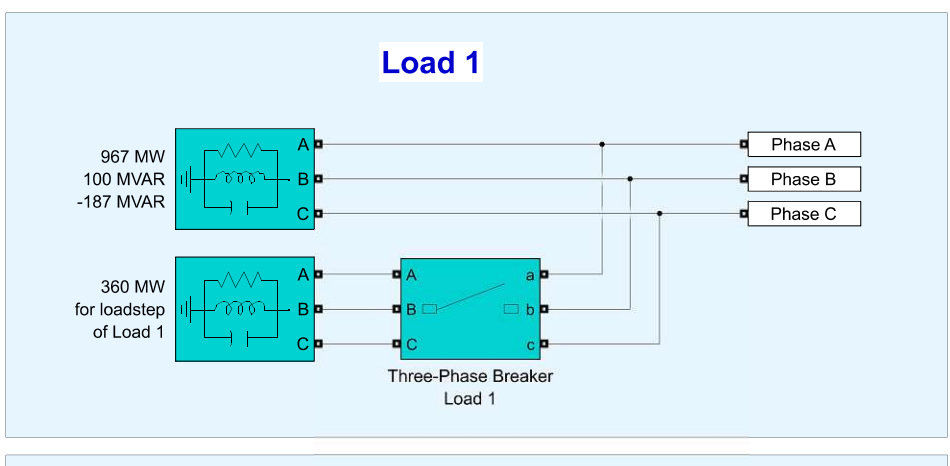


Figure 2.1: Illustration of the overall power grid topology of the Kundur-2-Area System.

the small-signal stability of the power systems through manipulation of the excitation voltage [5]. Their implementation is discussed in more detail in Section 2.1.2. Generator G4 is simulated without a PSS device to mimic not perfectly tuned components in the power grid, due to a natural lack of parameter knowledge or limited financial possibilities.

Figure 2.3 shows the differences of the PSS configurations between the generator units. Each turbine-generator unit is rated at 900 MVA and its detailed parameter sets are taken over from the MATLAB/Simulink example of the Kundur-2-Area System and listed in Tables 2.1 to 2.6. In the initial state the power grid is running at approximately 75% of its rated power capacity. The initial operating points of each generator can be found in Table 2.2.

Contrary to the power line distances and the generators, the grid loads are asymmetri-



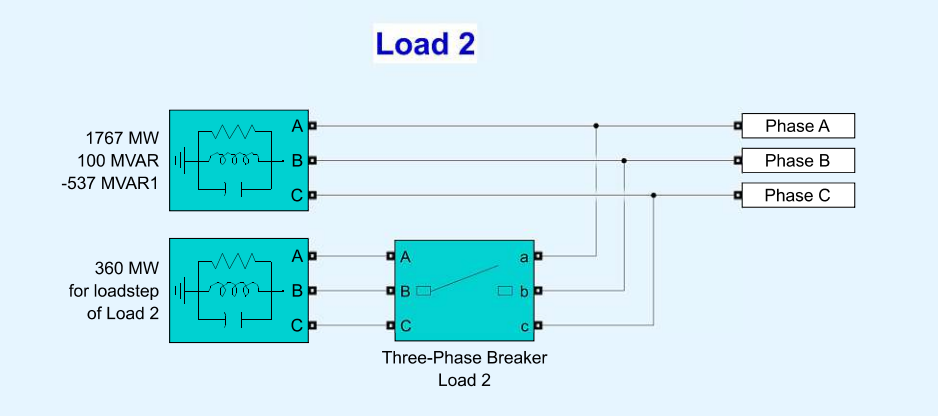
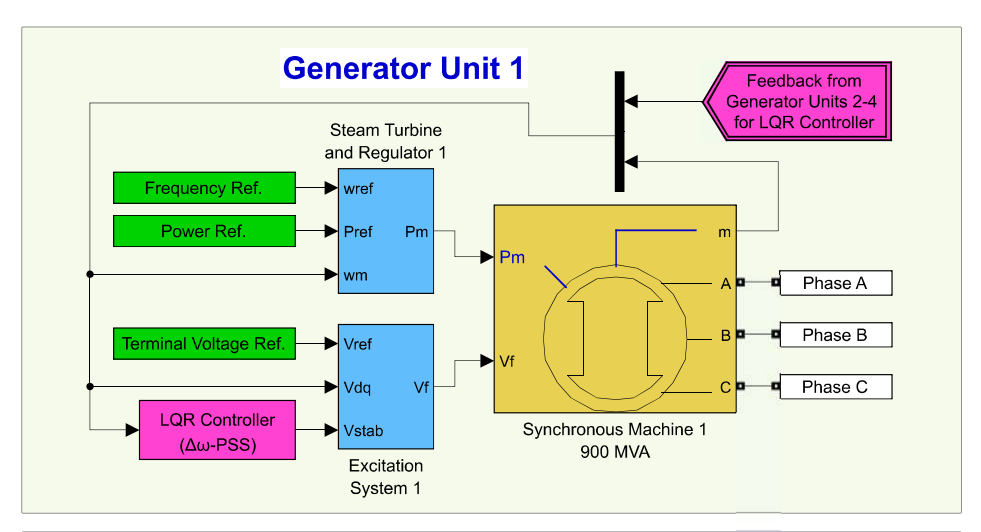
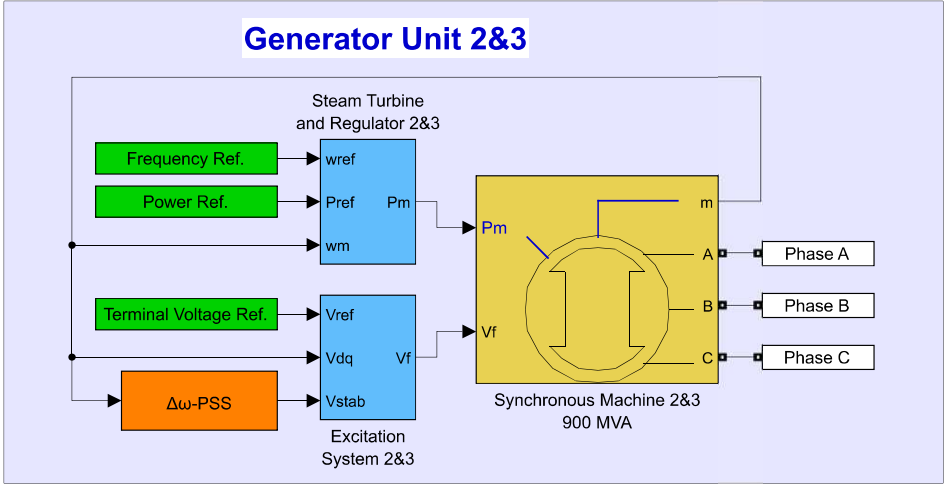


Figure 2.2: Illustration of the setup of the individual loads. MW denotes the active, MVAR the inductive reactive and -MVAR the capacitive reactive power ratings.

cally distributed. This leads to a permanent power transfer over the inter-area lines and lets us investigate the influence of the inter-area oscillations on the usage of the power transfer capacities. The rating of the loads is retained from the MATLAB/Simulink implementation of the Kundur-2-Area System. For the investigation of the transient grid behavior due to loadsteps the loads in Area 1 and in Area 2 are each composed by a base load and purely active switched load in.





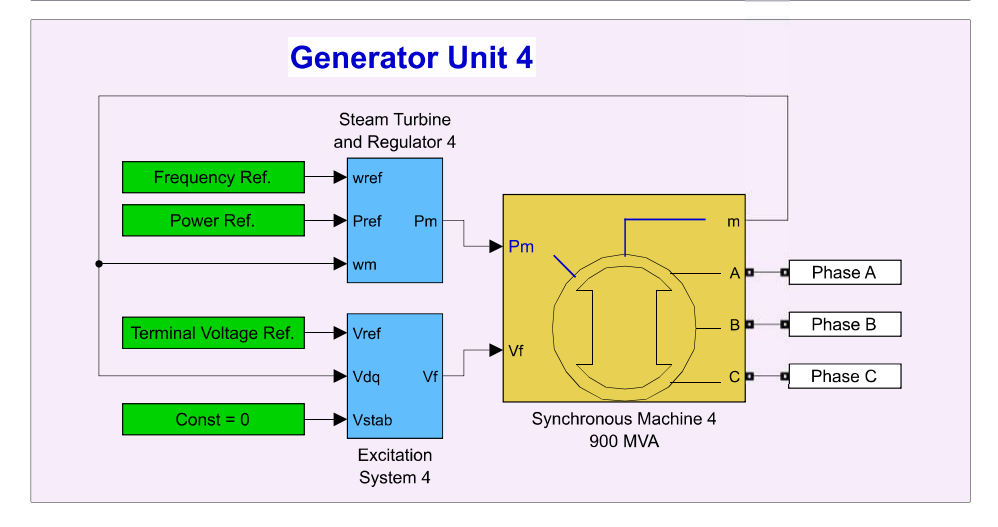


Figure 2.3: Illustration of the setup of the individual generator units.

# 2.1.1 Synchronous Machine Model

All of the four, as stated before, identical turbine-generator units use externally excited synchronous generators, which is the standard machine used in high power generator units. The state space model for such an electrical machine has two input variables. One is the power or torque coming from the turbine shaft and the other is the excitation voltage coming from an external supply (excitation system or exciter). The states corresponding to the synchronous machine model can be further subdivided into a mechanical model and an electrical model.

The mechanical model is composed by the equation of rotational inertia of the generator rotor, including torque components depending on the rotor angle and torque components depending on the rotor angular velocity. This leads to a second order differential equation, usually referred to as the swing equation [5, 19, 20]. As power grids usually have to run within relatively tight margins of voltage frequency, which, by a fixed scaling factor, corresponds to the generator rotational speed  $\omega_r$ , the equations of the mechanical generator model are often more conveniently written in per-unit deviation  $\Delta\omega_r$  from the synchronous rotating reference frame frequency  $\omega_0$ , so that we write

$$\Delta \dot{\omega}_r = \frac{1}{2H} (T_m - T_e - K_D \Delta \omega_r) \tag{2.1}$$

$$\dot{\delta}_r = \omega_0 \Delta \omega_r = \omega_r. \tag{2.2}$$

Here  $T_m$  denotes the torque input from the turbine shaft.  $T_e$  is the collective torque from the electromagnetic effects within the machine and thus from the conversion of mechanical power to electrical power. 2H corresponds to the per-unit moment of inertia of the rotor and  $K_D$  is an additional damping coefficient which is usually applied to account for oscillation damping losses [5, 2].

The electrical model captures the cross-correlating effects between the excitation voltage, the electrical loads and the resulting electrical fields between the generator stator and rotor, as well as the effects within the stator or the rotor. Those effects are usually simulated with a state space system using the electromagnetic fluxes in the synchronously rotating dq-reference frame as states. The exact formulation of this state space system depends on the rotor and stator construction and configuration as well as the required detail in the simulation. In this thesis we use the MATLAB/Simulink implementation of such a state space system assuming a round rotor, which is based on [20] and can be written

$$\frac{d\boldsymbol{\phi}}{dt} = -(\boldsymbol{R}\boldsymbol{L}^{-1} + \boldsymbol{W}(\omega_r))\boldsymbol{\phi} + \boldsymbol{v}.$$
 (2.3)

In this notation  $\phi = [\phi_q, \phi_d, \phi_{fd}, \phi_{kd}, \phi_{kq1}, \phi_{kq2}]^T$  is the state vector of flux linkages, **R** and **L** are the matrices of winding resistances and inductances, and  $W(\omega_r)$  is a matrix depending on the current rotor speed  $\omega_r$ . We note that the voltage vector  $\mathbf{v} = [v_q, v_d, v_{fd}, v_{kd}, v_{kq1}, v_{kq2}]^T$  is an input vector to this state space system of the electrical model. We will pick up on this fact again when discussing the network equation connecting the individual generators.

The previously mentioned electrical torque  $T_e$  of the mechanical generator equations can now be expressed as

$$T_e = \phi_d i_q - \phi_q i_d = \phi_d (\mathbf{L}^{-1} \boldsymbol{\phi})_q - \phi_q (\mathbf{L}^{-1} \boldsymbol{\phi})_d, \tag{2.4}$$

where the currencies  $i_d$  and  $i_q$  from the dq-reference frame can be expressed using the corresponding entries of the vector  $L^{-1}\phi$ .

Until now, we have just elaborated the equations to simulate a single generator unit. However, we still have to formulate the equations connecting those components to each other and form the power grid. This set of equations is usually referred to as the Power-Flow-equations. They can be derived from the first (currents) and second (voltages) Kirchhoff's law and depend on the structure of the power grid. Usually the number of independent grid nodes is smaller than the number of independent loops. For this reason, writing down the equations for the nodes from first Kirchoff's law is most often the preferred way. Using the node admittance matrix Y, we can write this set of equations as

$$I = YV. (2.5)$$

In this formulation V is the vector of phasor voltages to ground at the nodes  $1 \dots n$ , and I is the vector of the phasor currents added at the corresponding nodes  $1 \dots n$ . The entries of the phasor current vector I represent devices connected to the grid such as generators, converters or nonlinear loads. Whereas the entries of I corresponding to nodes without such devices, or connecting to constant admittance loads, which are included in the admittance matrix, are zero. The admittance matrix Y is composed of the diagonal entries  $Y_{i,i}$ , representing the self admittance of the node i, and the mutual admittances  $Y_{i,j}$  between the node i and j [5].

The resulting set of equations is a set of algebraic equations, which have to be fulfilled at any time throughout the simulation of the power grid. Together with the set of differential equations of the synchronous generator model, this forms a set of differentialalgebraic equations (DAE) [5, 2].

In some cases the system of DAEs describing the power grid can be mathematically transformed into a system of ordinary differential equations (ODE) [2, 6, 21]. This is also used by the Simulink back-end, when linearizing the power grid model. The resulting linear state space system therefore only consists of ODEs.

# 2.1.2 Additional Grid Components

# Steam-Turbine Regulator and Model

The steam turbine model itself is composed of a regulator model, regulating the steam flow into the turbine, and a model of the conversion of steam flow to mechanical shaft torque/power. A qualitative overview of the implementation is given in Fig. 2.4.

The regulator model consists of a servo-motor-driven valve model, with a limitation on opening and closing speed, as well as a limitation on the minimum and maximum opening state. To correct for control errors due to the speed limits, the regulator uses a feedback signal of the actual gate position to drive the steam gate into the desired position. Furthermore, it processes feedback information about the current rotor speed deviation via a tuned droop control [2].

The power of the steam flow then gets converted to mechanical power through a steam turbine. The steam turbine is modeled as a series of three stages. Each stage represents a separate fan and is modeled by a PT1 transfer function. A PT1 transfer function is a feasibly accurate model of a turbine stage for the purpose of this simulation [22]. It mainly aims to model the necessary pressure increase within a chamber in front of the turbine blades, before the increased steam flow results in an increase of torque. In this thesis 3 turbine stages are used in the simulation, referring to a high-, medium-, and low-pressure stage of the turbine [6, 23].

# Exciter

The exciter model processes feedback signals of the stator voltages in the dq-reference frame to estimate the terminal voltage of the synchronous generator and to make sure the requested terminal voltage is met. For the evaluation of the stator voltage signals a model of a terminal voltage transducer with load compensation is used. The model of this device is implemented by taking the root-mean-square of the stator voltages in the dq-reference frame and passing the resulting signal through a low-pass filter [5]. Additionally, the excitor model takes a so-called stabilization voltage into account. This stabilization voltage is a direct input from a PSS device. If no PSS device is installed in the generator unit, this stabilization voltage is constantly kept 0. Other than that, it only consists of a PT1 transfer function with an output saturation, approximating the response of a voltage regulation device. Figure 2.5 gives a general overview of the exciter model.

# Power System Stabilizer

As mentioned in the description of the grid topology, generators G2 and G3, as well as generator G1 for reference simulations, are equipped with a Power-System-Stabilizer device (PSS). The implementation of the PSS devices used in this thesis use the deviation of the local generator frequency compared to the nominal grid frequency as input. Over a series of carefully tuned transfer functions [5, 6] a value for the stabilization voltage is calculated and directly passed to the exciter model. A block diagram of the used PSS model is shown in Fig. 2.6.

# Load

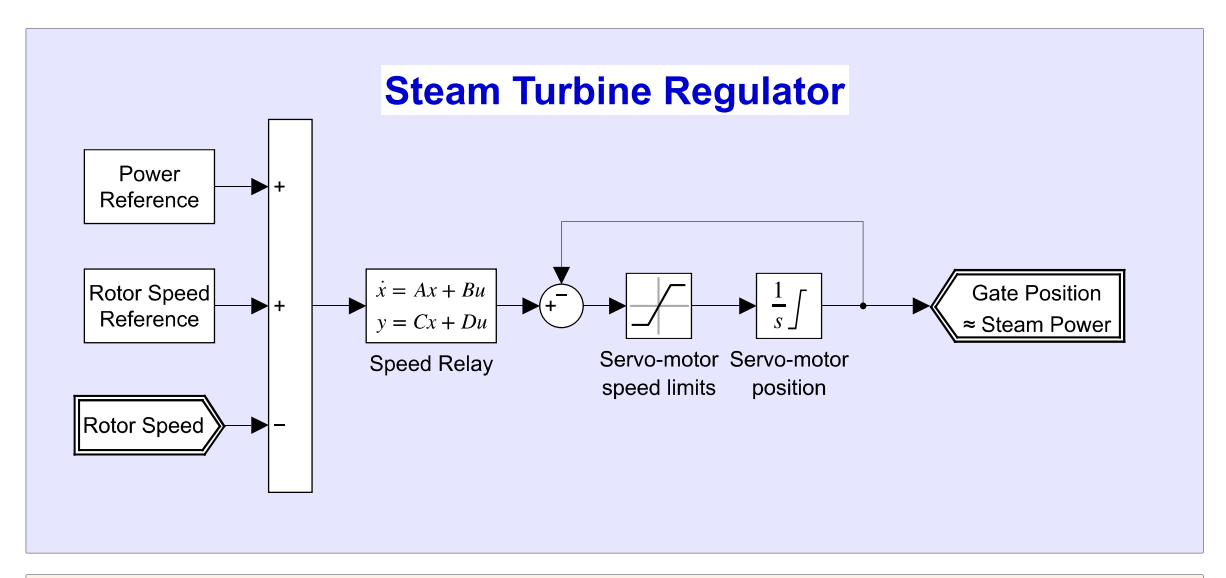
The dynamic load model is implemented as very fast PT1 transfer functions on the real and imaginary parts of the current pointers. This is important to obtain states through the linearization of the grid model, which correspond to the active and reactive loads. For the simulations in this thesis the Three-Phase Dynamic Load - block of the Simscape/Electrical/Specialized Power System Toolbox is used. In the cases where no states corresponding to loads in the linearized power grid model were necessary the Three-Phase Parallel RLC Load - block and the Three-Phase Breaker - block from the same library, as the dynamic load block, were used.

# Transformers and Power Lines

There are two further grid components in the Simulink power grid model. One of which are the transformers close to the generators, which transform the 20KV terminal voltage of the generators to the 220kV voltage of the power lines. They are modeled as passive elements with a resistance and an inductance. For more detail we refer to the Simulink documentation of the Three-Phase Transformer (Two Windings) model [24].

The last grid component to discuss are the power lines. Obviously the simulation model of the power lines has to consider an electric resistance per unit length. However, a more detailed simulation model, especially for long power lines, also has to take an additional impedance per unit length into account.

For more detailed information on those components it is again referred to the Simulink documentation of the Three-Phase PI Section Line - and the Distributed Parameter Line - block [25].



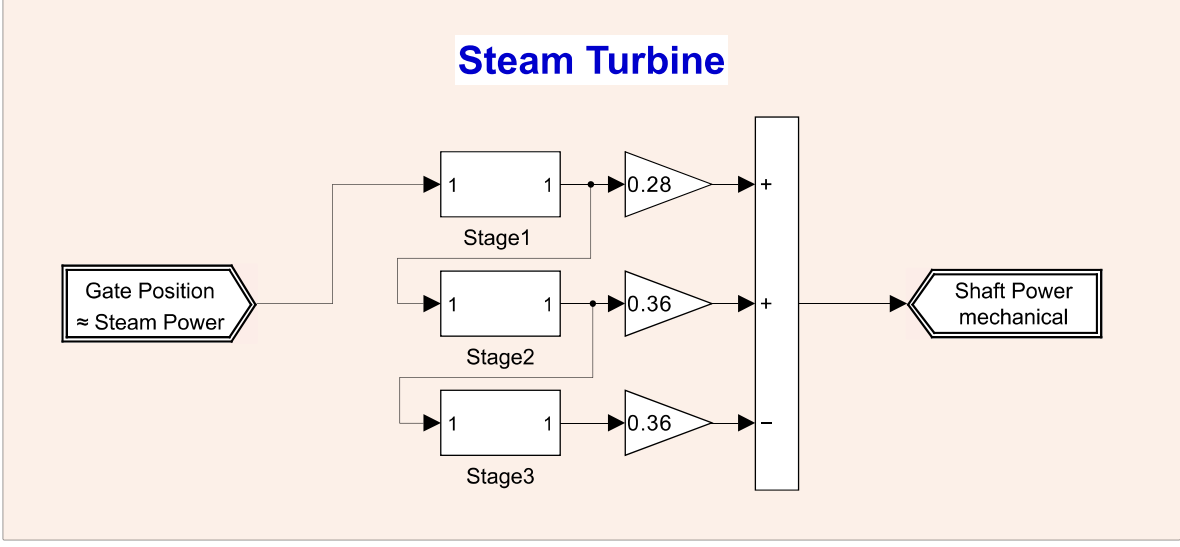


Figure 2.4: Block diagram of the Steam Turbine Regulator and Model.

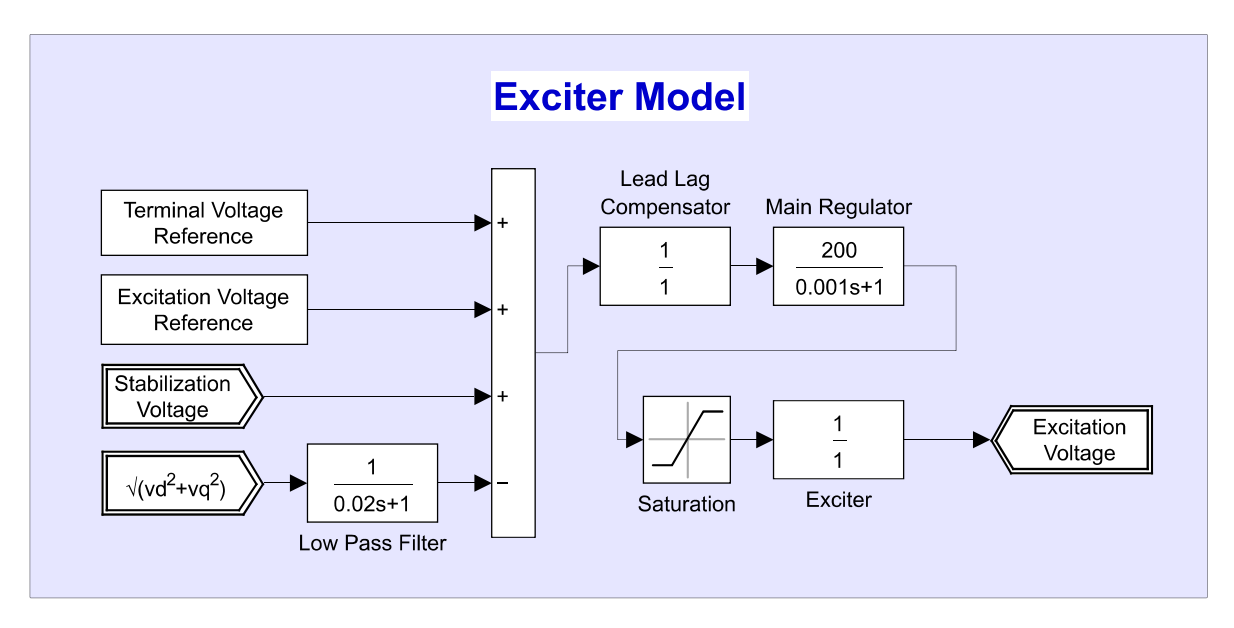


Figure 2.5: Block diagram of the Exciter Model.

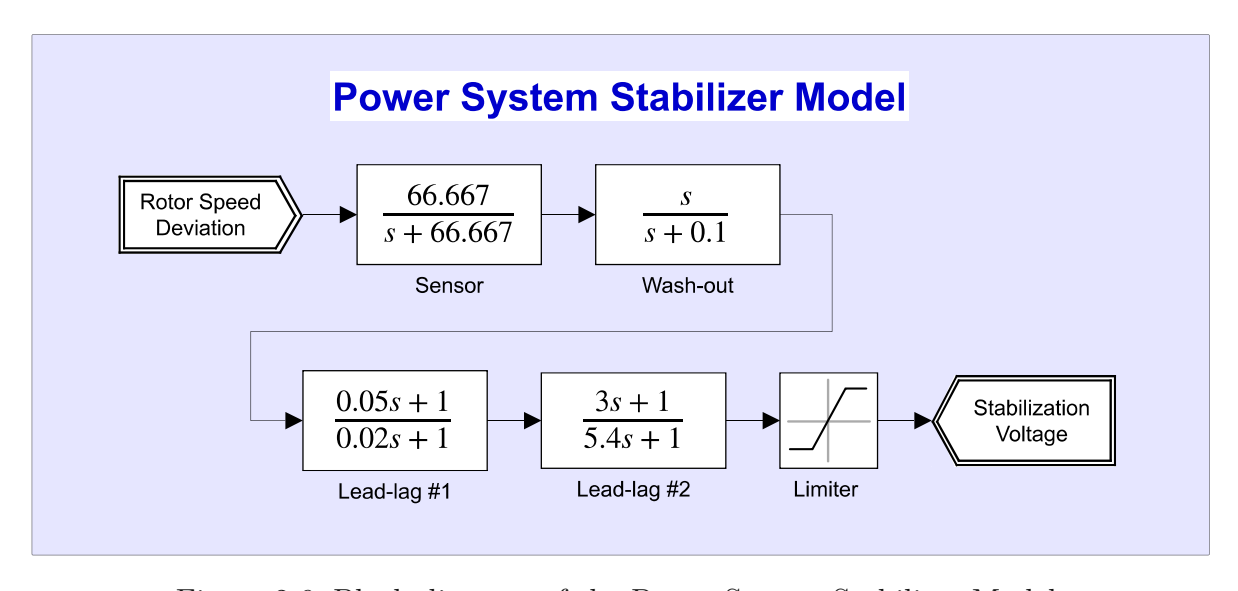


Figure 2.6: Block diagram of the Power System Stabilizer Model.

# 2.1.3 Simulink/Simscape Model of Power Grid

To ensure the power grid model used for this thesis can be replicated by others we declare all parameter settings used in the Simulink models of the discussed grid components in Tables 2.1 to 2.6.

Parameters of the Synchronous Generator Model		
Mechanical input	Mechanical power Pm	
Rotor type	Round	
Nominal power, line-to-line voltage, frequency [ Pn(VA) Vn(Vrms) fn(Hz) ]	[900e6 20000 60]	
Reactances [ Xd Xd' Xd" Xq Xq' Xq" XI ] (pu)	[ 1.8 0.3 0.25 1.7 0.55 0.25 0.2 ]	
Time constants: d axis	Open-circuit	
Time constants: q axis	Open-circuit	
Time constants: [ Tdo' Tdo" Tqo' Tqo" ] (s)	[ 8 0.03 0.4 0.05 ]	
Stator resistance Rs (pu)	0.0025	
Inertia coefficient, friction factor, pole pairs [ H(s) F(pu) p()]	[6.5 0 4]	
Initial conditions	[ 0 -31.4247 0.784453	
[ dw(%) th(deg) ia,ib,ic(pu)	0.784453 0.784453 2.7401	
pha,phb,phc(deg) Vf(pu) ]	-117.26 122.74 1.83395 ]	
Generator type	PV	
Active power generation P (W)	[ 700e6 ]	
Minimum reactive power Qmin (var)	-inf	
Maximum reactive power Qmax (var)	inf	

Table 2.1: Parameters used to configure the Simulink-block of the Synchronous Generator Model.

As mentioned before, the set of equations needed to describe a power grid is composed of differential and algebraic equations, making it a DAE system. To incorporate those algebraic equations into a Simulink simulation, one needs a suitable solver. This is what the Simscape engine provides. In rough terms the voltage and current signals are not transferred between components using standard Simulink signal links, but are mapped into the power system solver, which takes care about the algebraic power flow equations corresponding to the physical links [26].

Parameters of the Steam-Turbine Regulator and Model		
Generator type	Tandem-compound (single mass)	
Regulator gain, perm. droop, dead zone [ Kp Rp(pu) Dz(pu) ]	[10.050]	
Speed relay and servo-motor time constants [ Tsr Tsm ] (s)	[0.001 0.15]	
Gate opening limits [ vgmin,vgmax (pu/s) gmin,gmax (pu)]	[-0.1 0.1 0 4.496]	
Nominal speed of synchronous machine (rpm)	3600	
Steam turbine time constants [ T2 T3 T4 T5 ] (s)	[ 0 10 3.3 0.5 ]	
Turbine torque fractions [ F2 F3 F4 F5 ]	[ 0 0.36 0.36 0.28 ]	
Initial power Pm0 (pu) Generator Unit 1	0.7778	
Initial power Pm0 (pu) Generator Unit 2	0.7777	
Initial power Pm0 (pu) Generator Unit 3	0.798889	
Initial power Pm0 (pu) Generator Unit 4	0.7778	

Table 2.2: Parameters used to configure the Simulink-block of the Steam Turbine and Regulator Model.

Parameters ot the Exciter Model		
Low-pass filter time constant Tr(s)	[ 20e-3 ]	
Regulator gain and time constant [ Ka() Ta(s) ]	[ 200 0.001 ]	
Exciter [ Ke() Te(s) ]	[10]	
Transient gain reduction [ Tb(s) Tc(s) ]	[00]	
Damping filter gain and time constant [ Kf() Tf(s) ]	[00]	
Regulator output limits and gain [ Efmin, Efmax (pu), Kp() ]	[-12.3 12.3 0]	
Initial values of terminal voltage and field voltage [ Vt0 (pu) Vf0(pu) ]	[ 1 1.83395 ]	

Table 2.3: Parameters used to configure the Simulink-block of the Exciter Model.

Parameters of the PSS Model		
Sensor time constant:	[ 15e-3 ]	
Gain	30	
Wash-out time constant:	10	
Lead-lag #1 time constants: [ Tnum Tden ]	[ 50e-3 20e-3 ]	
Leag-lag #2 time constants: [ Tnum Tden ]	[35.4]	
Output limits: [ VSmin VSmax ]	[ -0.15 0.15 ]	
Initial input	0	

Table 2.4: Parameters used to configure the Simulink-block of the Power System Stabilizer Model.

Parameters of the Transformers		
Winding 1 connection (ABC terminals)	Delta (D1)	
Winding 2 connection (abc terminals)	Yg	
Туре	Three single-phase transformers	
Nominal power and frequency [ Pn(VA) , fn(Hz) ]	[ 900e6 60 ]	
Winding 1 parameters [ V1 Ph-Ph(Vrms) , R1(pu) , L1(pu) ]	[ 20e3 1e-6 0 ]	
Winding 2 parameters [ V2 Ph-Ph(Vrms) , R2(pu) , L2(pu) ]	[ 230e3 1e-6 0.15 ]	
Magnetization resistance Rm (pu)	500	
Magnetization inductance Lm (pu)	500	

Table 2.5: Parameters used to configure the Simulink-block of the Transformer Model.

Parameters of the Power Lines		
Positive- and zero-sequence resistances (Ohms/km) [ r1 r0 ]	[ 0.0529 1.61 ]	
Positive- and zero-sequence inductances (H/km) [ l1 l0 ]	[ 0.00140318 0.0061 ]	
Positive- and zero-sequence capacitances (F/km) [ c1 c0 ]	[ 0.00245557 5.2489e-9 ]	
Frequency used for rlc specification (Hz)	60	

Table 2.6: Parameters used to configure the Simulink-block of the Power Line Model.

# 2.1.4 Phasor Simulation

At this point we have to mention the simulation mode with which the simulations of the power grid model were carried out. The Simulink/Simscape not only allows simulation by continuous or discrete time integration, but also provides a so-called phasor, or frequency-and-time simulation mode. To apply this phasor simulation mode, the model has to have a single nominal frequency. All of the model variables are then defined with respect to this nominal frequency. This allows the solver to increase the step size compared to the time-based mode. Consequently, when applicable, the phasor simulation mode speeds up the simulation. However, we have to consider that this speed-up comes with decreased simulation accuracy of high frequency effects.

But as the targeted frequency oscillations of this thesis are in the range of 0-5Hz, and therefore even much slower than the nominal grid frequency (60Hz), the phasor simulation mode is assumed to be sufficient and was used in all simulation runs.

We also have to point out, that the simulation mode selection changes the implementation of the grid components. Although we consider the effects of those changes negligible for the simulation results, they can have other impacts on the following presented methods for generating model linearizations. We declare that we tested and used all of the methods from Sections 2.1.5 and 2.1.6 only on implementations using the phasor simulation mode.

For more detailed information on the phasor or frequency and time simulation mode we refer to the MATLAB/Simulink documentation [27].



# 2.1.5 Linearizing Simulink Models

To analyze our power grid system in terms of observability, controllability or to design a feedback controller for it, we want to use the immense range of linear analysis tools. However, up until now we just set up an nonlinear Simulink simulation model, but do not have a linearized system representation at hand. For these cases MATLAB/Simulink provides an extraordinarily practical tool, which lets us easily generate linearizations of Simulink models at valid operating points. This also works for simulations modeled within the Simscape framework. This feature can be found in the so-called 'Model Linearizer App' which also provides a graphical user interface [28].

For our application we mainly need to know how to define an operating point for our linearization, how the states of our linearization are found, and how the software handles certain blocks like signal-limitation blocks.

First of all we provide a set of initial conditions to the simulation, which might be close enough to an actually stable operating point, but not exact. Therefore, we expect to need an initialization period at the start of our simulation, to find an actual stable operating point. After this initialization phase of the simulation, we can linearize the system and get a linear model which is able to run stable at the current operating point. For this reason, we use the feature 'Linearize at timestep', which lets us define a certain point in time, within the simulation timespan, at which the model gets linearized. Here we chose to linearize at 9 second into the simulation, which is well after the initialization phase and before any loadsteps.

Next, we have to care about blocks, which introduce nonlinearities into our model. Those blocks are usually treated as simple gain blocks throughout the linearization, where the gain factor is evaluated from the current gain of the nonlinearity. This also applies for signal-limitation blocks. We can notice that when, for example, we can increase the steam flow to the steam turbine much faster in the linearized model, than we would be able to do in the nonlinear Simulink model. During the subsequent analysis of the linear model, we have to keep in mind that the linearization, therefore, might suggest a significantly different behavior of the linear model compared to the nonlinear model.

Last but not least, we need to know exactly what blocks from our model become states in state space representation. We need to know this, because we want to provide a state feedback, which means to draw a signal link from every block, creating a state, to the controller we want to design. In short terms every output of an integrator-block and every state of a state-space subsystem is a state of the overall model. However, especially with state-space subsystems we do not have direct access to the inherent state, but only to the output of the block. This distinct difference becomes very important if a state-space subsystem has a C-matrix which is not an identity matrix or has a nonzero D-matrix (assuming a state-space system  $\dot{x} = Ax + Bu$  and y = Cx + Du). The output of such a block obviously does not correlate with the state of the block,

and we have to account for that to generate a meaningful feedback signal.

TU **Bibliothek**, Die approbierte gedruckte Originalversion dieser Diplomarbeit ist an der TU Wien Bibliothek verfügbar wer knowledge hub The approved original version of this thesis is available in print at TU Wien Bibliothek.

# 2.1.6 Handling feed-through Systems

As previously discussed, some model states of the Simulink model are not directly available as we can only access the output of blocks that introduce states to our model. However, in the following proceedings we want to apply a full state feedback controller to our Simulink model, hence we have to either provide state feedback signals or account for the difference between model states and block outputs within the controller gains. If we place so-called 'Output Measurement'-points at every feedback signal for our controller, the 'Model Linearizer App' generates an output y and the corresponding row of the C-matrix of the linearized system. At this point we might notice that the linearized system has rows of its C-matrix which contain more than just one single nonzero entry and might also be different from 1. These rows indicate states that are not directly accessible in our Simulink model. There are two general approaches to resolve the mismatch of model state signals to block output signals. The first one is to change the implementation of the Simulink model in order to obtain direct access to the model state signals. The other approach, which was chosen for this thesis, is to introduce a similarity transformation for the linearized system so the states of the transformed linearized system correspond to the block outputs available in the Simulink model. This approach therefore accounts for the not directly available states within the controller gains, which are received through methods on the transformed linearized model.

In the next section we will discuss how to construct this similarity transformation mentioned above. We already noted how we gather information about the composition of our available block outputs by placing 'Output Measurement' points on all our feedback signals. After linearization, this gives us a model with exactly as many outputs as states.

$$\dot{\boldsymbol{x}}_{\text{lin}} = \boldsymbol{A}_{\text{lin}} \boldsymbol{x}_{\text{lin}} + \boldsymbol{B}_{\text{lin}} \boldsymbol{u} \quad \text{and} \quad \boldsymbol{y}_{\text{meas}} = \boldsymbol{C}_{\text{lin}} \boldsymbol{x}_{\text{lin}}$$
 (2.6)

We now want to transform this linear system into a system where the states corresponding exactly to the outputs of the original system, so that

$$\dot{\boldsymbol{x}}_{\mathrm{sig}} = \boldsymbol{A}_{\mathrm{sig}} \boldsymbol{x}_{\mathrm{sig}} + \boldsymbol{B}_{\mathrm{sig}} \boldsymbol{u}$$
 and  $\boldsymbol{y}_{\mathrm{meas}} = \boldsymbol{C}_{\mathrm{sig}} \boldsymbol{x}_{\mathrm{sig}}$  (2.7)

whereas  $y_{\text{meas}} = x_{\text{sig}}$  shall hold true  $(\Rightarrow C_{\text{sig}} = I)$ .

This requirement immediately leads us to the required similarity transformation matrix,

$$C_{\text{lin}}x_{\text{lin}} = C_{\text{sig}}x_{\text{sig}} = x_{\text{sig}} \quad \Rightarrow \quad x_{\text{lin}} = C_{\text{lin}}^{-1}C_{\text{sig}}x_{\text{sig}} = C_{\text{lin}}^{-1}x_{\text{sig}}$$
 (2.8)

which is the C-matrix of the original linear system (or its inverse respectively).

By inserting this similarity transformation into the originally linearized state space system Eq. (2.6)

$$C_{\text{lin}}^{-1}\dot{\boldsymbol{x}}_{\text{sig}} = \boldsymbol{A}_{\text{lin}}\boldsymbol{C}_{\text{lin}}^{-1}\boldsymbol{x}_{\text{sig}} + \boldsymbol{B}_{\text{lin}}\boldsymbol{u} \quad \Rightarrow \quad \dot{\boldsymbol{x}}_{\text{sig}} = \boldsymbol{C}_{\text{lin}}\boldsymbol{A}_{\text{lin}}\boldsymbol{C}_{\text{lin}}^{-1}\boldsymbol{x}_{\text{sig}} + \boldsymbol{B}_{\text{lin}}\boldsymbol{u}$$
 (2.9)

we can evaluate the transformations of the original A and B matrices

$$A_{\text{sig}} = C_{\text{lin}} A_{\text{lin}} C_{\text{lin}}^{-1}$$
 and  $B_{\text{sig}} = C_{\text{lin}} B_{\text{lin}}$  (2.10)

and can define a matrix  $C_{\mathrm{sig}}$  according to our needs.

The transformed linear system allows us to design a linear controller and be sure the controller can handle the block outputs as state feedback signals when applied on the Simulink model.

# 2.1.7 Loadstep Scenarios

In this section we define the testing scenarios used to evaluate the performance of the designed controllers. We defined two scenarios for different purposes. The first scenario is set up with a single loadstep to evaluate the damping performance of the controller. The second defined scenario aims to evaluate the controller behavior on a wide range of operating conditions. Hence we use it to investigate the controller stability throughout a broader range of nonlinear system behavior. For this reason, the second scenario contains a series of loadsteps from both loads as well as changes of the generator power output references.

The single loadstep scenario includes a sudden increase of load at t = 10 sec (after an initialization phase of the simulation) introduced through either Load 1 or Load 2. The power demand increase accounts for approximately 13% (360MV) of the overall grid rating, which increases the overall grid capacity utilization from 75% to 88%. This is set up to put relatively high stress on the grid and force a significant grid frequency drop. Following the load increase the reference power is only increased at generator 2 with two consecutive 5\% steps at t = 15s and t = 20s.

This unsophisticated compensation of the overall power balance was done for two reasons.

The first reason is that reference power changes on the generator unit setup of this thesis only effect the grid frequency very slowly. This is mostly due to the limitation on the steam flow rate of change in the nonlinear model, which is necessary to consider the structural loads on the steam pipes. Hence, the resulting impact of reference power changes can be considered too slow to effect the targeted frequency oscillations. Therefore neglecting a reference power change during a short period after the loadstep does also barely limit the damping performance. The second reason is to keep the complexity of the model down by avoiding an additional controller for the reference power with its own tuning. Furthermore, one might then also consider limitations of the operational framework, like different reserve capabilities of the individual plants. All of which can be neglected due to the first reason.

The scenario for testing a wider range of operating conditions contains a series of loadsteps from both loads as well as changes of the generator power output references. The loadsteps are timed in a way that they take the power grid from approximately 50% of the grid capacity rating up to 100% during which also different power transfer loads from the inter-area power line connection are tested.

The output power references of the four generators are adapted with a slight timeshift to the loadstep. The order of magnitude of reference changes is chosen to approximately match  $P_{\text{input}} = P_{\text{output}}$ , with  $P_{\text{input}}$  being the sum of all power inputs and  $P_{\text{outputs}}$  the sum of all power consumptions. Whereas this is a feasible assumption in general, it is also necessary to keep the grid frequency within a feasible range.

# Controllability and Observability of Modes

# 2.2.1 Identification of Oscillation Modes

In the following section we discuss the methods used in this thesis to identify and further analyze certain oscillation modes. This will include identification of poles based on an approximate measure of their eigenfrequency, or the composition of their corresponding eigenvector. We will further discuss the theoretical measures of how well we can actuate on some oscillation modes as well as how well we are able to recognize them through specific sets of feedback signals.

As the target of this work is to design a controller which specifically dampens oscillations between generators of a power grid, and we already have a linear system representation of this power grid, we first have to identify the poles or eigenvalues of this linear system responsible for the unwanted oscillations. Once we have identified those poles, we can design a control law, which decisively moves those poles in a way, so that the respective oscillation modes of our system become much more damped.

To identify the eigenvalues of the inter-area oscillation mode, we can get a first hint by measuring the frequency of the observable oscillations in the simulation results of a loadstep response from the original (reference) power grid configuration, Fig. 2.7.

A measurement of approximately 0.63...0.67 Hz corresponds only to a slightly damped polepair located at  $\pm 3.9i \dots \pm 4.2i$ . Therefore assuming the poles at  $-0.26 \pm 4.04i$ (frequency f = 0.64 Hz and damping ratio  $\zeta = 0.06$ ) are responsible for this oscillation mode is reasonable, as there are no other nearly as undamped poles nearby, see Fig. 2.8. The next most undamped poles in a similar frequency range are at approximately  $-2.23 \pm 8.00i$  (f = 1.32 Hz,  $\zeta = 0.26$ ) and  $-1.79 \pm 7.85i$  (f = 1.28 Hz,  $\zeta = 0.22$ ). For further investigation of the oscillation modes corresponding to those three pole pairs we examine their eigenvectors. A large entry, in relation to its overall length, in the eigenvector tells us the corresponding state of our system is strongly involved in the oscillation mode under consideration. On the other hand, a small entry, compared to its overall length, in the eigenvector means the corresponding state is not much involved [29]. In the present case of the oscillation between generators in a power grid, we might not be particularly interested in the exact states corresponding to large entries of the eigenvectors, but more interested in the area or generator unit we can assign the specific state to. In Fig. 2.9 we see that the eigenvector corresponding to the eigenvalue at  $-2.23 \pm 8.00i$  has very prominent main directions towards the generator units G1 and G2 compared to its remaining main directions. Similarly, the eigenvector of the eigenvalue  $-1.79 \pm 7.85i$  has very distinct main directions towards the generator units G3 and G4. This lets us allocate those two eigenvalues to the in-area-1 and in-area-2 oscillations respectively. In contrast, the eigenvector corresponding to the eigenvalue

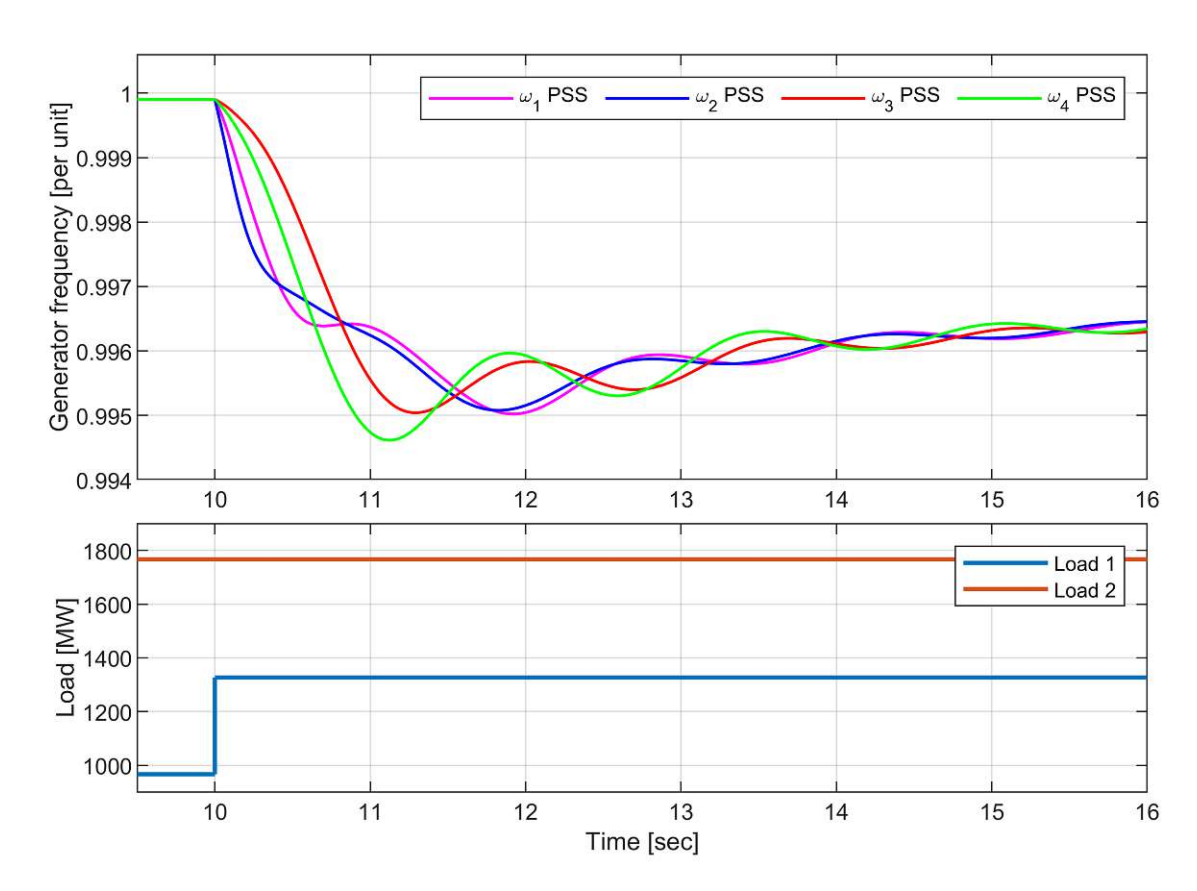


Figure 2.7: Rotor angular speeds of generators G1-G4 after a loadstep on the original power grid configuration. In this configuration a PSS device is installed in the generator units G1, G2 and G3.

 $-0.26 \pm 4.04i$  has much more balanced main direction shares towards all four generator units. Therefore, we can allocate this eigenvalue to the inter-area oscillation mode.

Furthermore we can also analyze the behavior of specific state variables when starting a simulation of the linear model from specific initial values. If we make sure to start our simulation exactly on an oscillation plane corresponding to an eigenvalue  $\lambda_i$ , the state space system does not leave this oscillation plane throughout the simulation. We can then analyze the behavior of state variables during such a simulation and observe in what way each variable is involved in the oscillation corresponding to  $\lambda_i$ .

To start the simulation exactly on a specific oscillation plane we recall that, for a pair of complex conjugate eigenvalues  $\lambda_i$  and  $\lambda_i$ , the oscillation plane is spanned by the corresponding pair of complex conjugate eigenvectors  $\phi_i$  and  $\phi_i$ .

Therefore we can choose an arbitrary linear combination of the real and imaginary parts of  $\phi_i$  to start the simulation exactly on the oscillation plane of  $\lambda_i$ . In Fig. 2.10 we

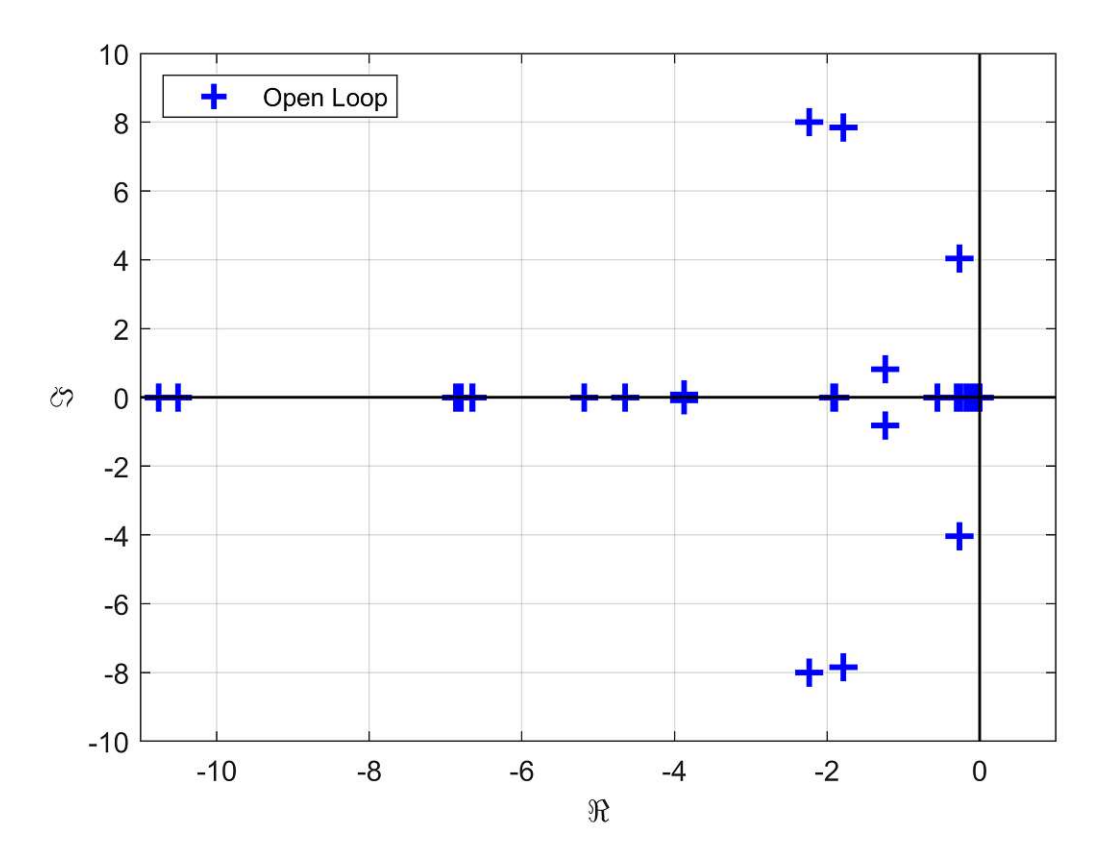


Figure 2.8: Eigenvalues of the linearized power grid system for an open-loopinput at the stabilization voltage of the generator unit G1.

compare the angular velocity deviations of the four generator units by two throughout such simulations for the three most prominent pole pairs. In those plots we can clearly distinguish between angular velocities which increase and decrease together and angular velocities which behave in an opposing manner. The former indicates that the respective generators are oscillating in sync with each other, whereas the latter behavior indicates generators oscillating against each other for the specific mode. For instance the graph for the eigenvalue at  $-0.26 \pm 4.04i$ , we observe that  $\Delta\omega_1$  is oscillating in phase with  $\Delta\omega_2$  and  $\Delta\omega_3$  is in phase with  $\Delta\omega_4$  as well, whereas  $\Delta\omega_1$  is oscillating against  $\Delta\omega_3$  and  $\Delta\omega_4$ . Hence, this is the eigenvalue corresponding to the inter-area oscillation mode. For the in-area-1 and in-area-2 modes we can also observe oscillation planes close to perpendicular to a specific axis. This indicates that the specific corresponding generator does not participate at all in the oscillation mode under consideration. For example we see that  $\Delta\omega_1$  and  $\Delta\omega_2$  both do not participate in oscillations on the oscillation planes of the eigenvalue  $-1.79 \pm 7.85i$ , but only  $\Delta\omega_3$  and  $\Delta\omega_4$  do. This lets us conclude that

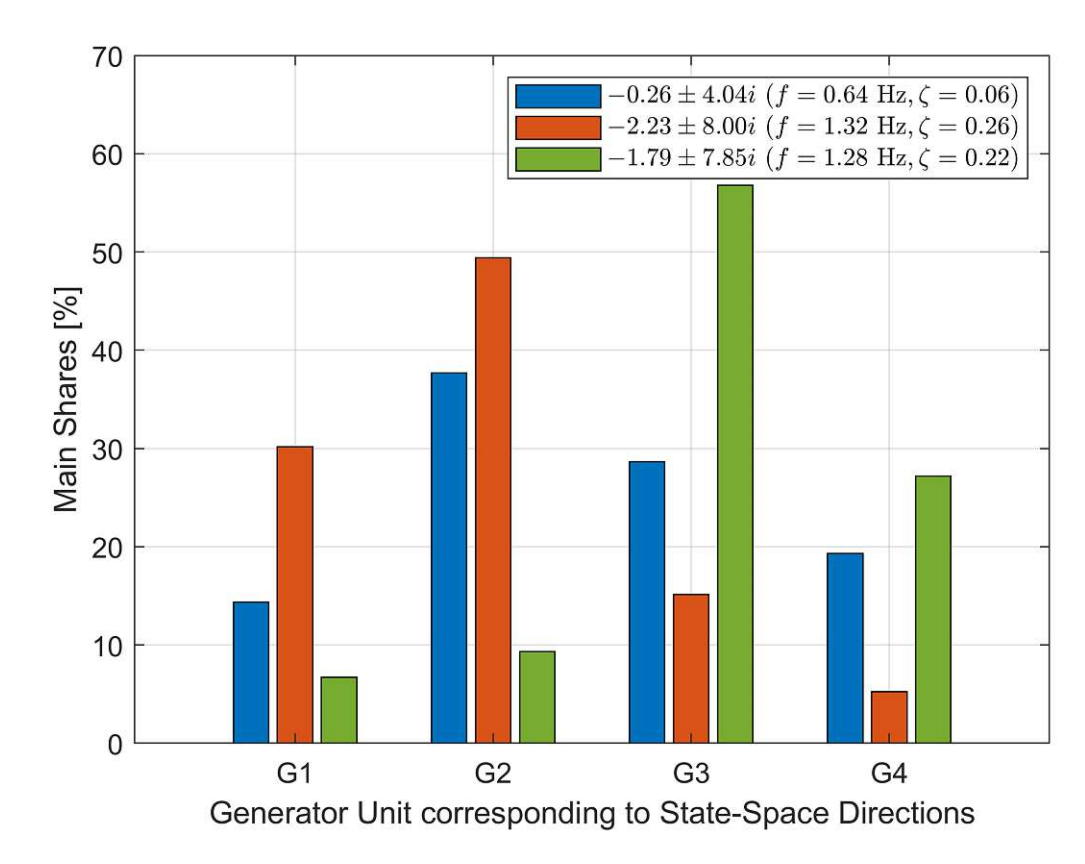


Figure 2.9: Proportional shares of the most prominent eigenvector directions from the eigenvectors corresponding to the most critical eigenvalues. The eigenvector directions can be allocated to the four different generator units via their corresponding states.

the eigenvalue corresponds to the in-area-2 oscillation mode.

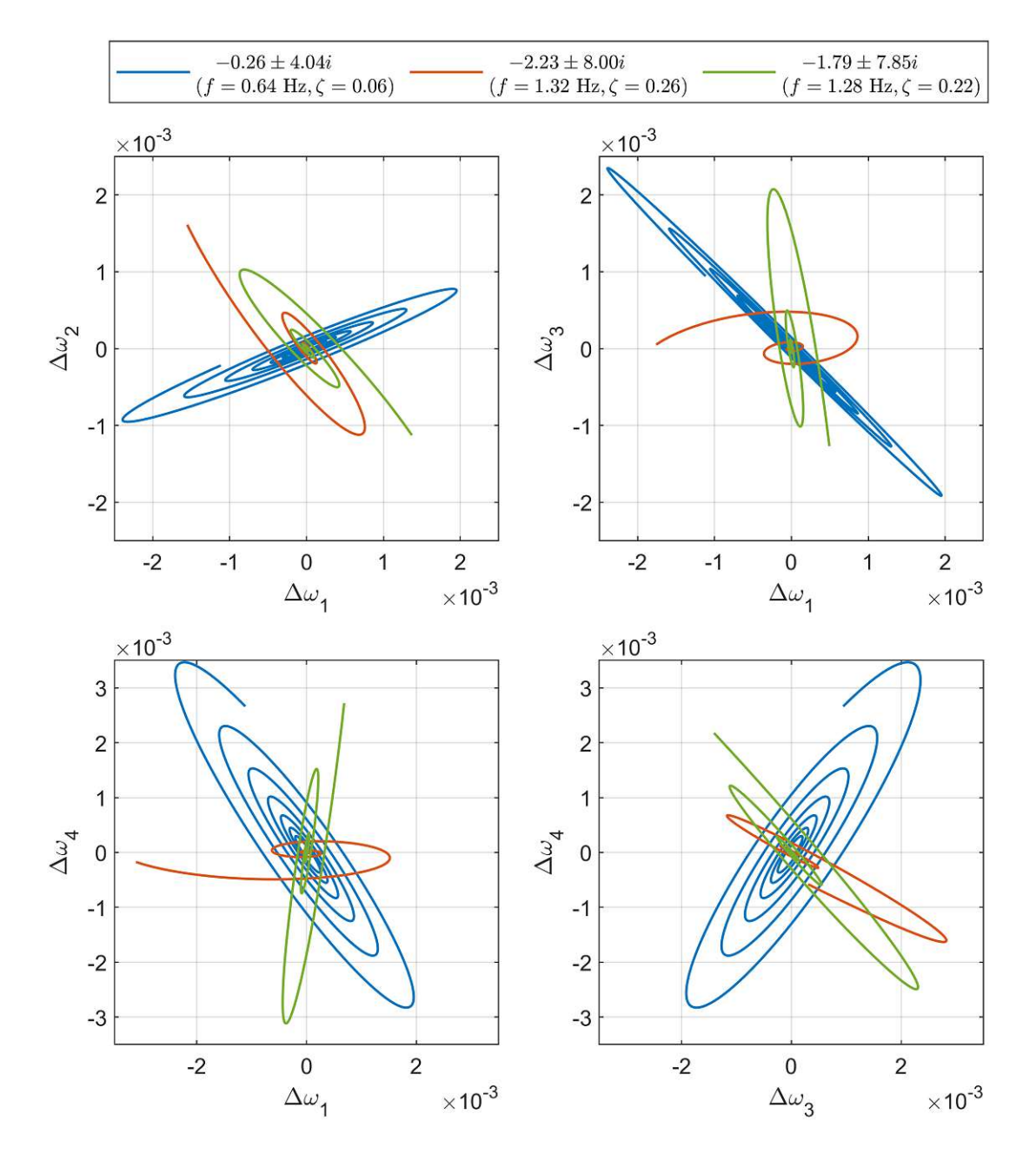


Figure 2.10: Rotor speeds of the different generator units after initializing simulations on the oscillation planes corresponding to the most critical eigenvalues.

### 2.2.2 Modal State Transformation

In this section we elaborate more on measures of how well we can influence modes with specific inputs (controllability) and how well we can recognize modes with specific feedback signals (observability) respectively.

The basic approach to this is to find a similarity transformation for our state space system, which lets us interpret the B- and C-matrix of our system with respect to the modes under consideration. For such a similarity transformation we can use the right or left eigenvector matrices,  $\Phi_{\rm r}$  or  $\Phi_{\rm l}$ , as transformation matrices [30, 31, 32].

For demonstration, the right eigenvector matrix  $\Phi_{\rm r}$  is defined as the solution to the eigenvalue problem  $A\Phi_{\rm r}=\Phi_{\rm r}\lambda$ . If all  $\lambda_i$  have a geometric multiplicity  $m_{\rm geo.}$  equal to their algebraic multiplicity  $m_{\rm alg.}$ ,  $\boldsymbol{A}$  is called diagonalizable and  $\boldsymbol{\lambda}$  is a diagonal matrix of the eigenvalues of A. If an eigenvalue has  $m_{\rm geo.} < m_{\rm alg.}$ , we have to introduce generalized eigenvectors to find suitable transformation matrices. As a result, we have to consider blocks of the Jordan canonical form in the transformed system matrix [30, 31]. However, since we do only investigate the in-area-1, in-area-2 and inter-area eigenvalues, which have  $m_{\text{geo.}} = m_{\text{alg.}} = 1$ , those eigenvalues are transformed to completely decoupled states in the modal state space system. Since this decoupling allows the application of the following methods on the eigenvalues under consideration, we do not consider eigenvalues with  $m_{\rm geo.} < m_{\rm alg.}$  any further in our proceedings.

With  $x = \Phi_{\rm r} z$  the state space system transforms to

$$\dot{z} = \underbrace{\Phi_{r}^{-1} A \Phi_{r}}_{=\tilde{A} = \lambda} z + \Phi_{r}^{-1} B u \quad \text{and} \quad y = \underbrace{C \Phi_{r} z}_{=\tilde{C}} + D u.$$
(2.11)

Likewise,  $\boldsymbol{x} = \boldsymbol{\Phi}_1^{-T} \boldsymbol{z}$  transforms the state space system to

$$\dot{\boldsymbol{z}} = \underbrace{\boldsymbol{\Phi}_{1}^{T} \boldsymbol{A} \boldsymbol{\Phi}_{1}^{-T}}_{=\tilde{\boldsymbol{A}} = \lambda} \boldsymbol{z} + \underbrace{\boldsymbol{\Phi}_{1}^{T} \boldsymbol{B}}_{=\tilde{\boldsymbol{B}}} \boldsymbol{u} \quad \text{and} \quad \boldsymbol{y} = \boldsymbol{C} \boldsymbol{\Phi}_{1}^{-T} \boldsymbol{z} + \boldsymbol{D} \boldsymbol{u}. \tag{2.12}$$

As stated before, the transformed matrix  $\boldsymbol{A}$  of the modal systems  $\boldsymbol{z}$  contains only eigenvalues or Jordan canonical blocks on its diagonal. Hence, this representation of the system, lets us investigate all the eigenvalues with  $m_{\rm geo.}=m_{\rm alg.}$  separately. We further notice, that the entries  $B_{i,j}$  are composed by  $\phi_{l,i}^T B_j$ , where  $\phi_{l,i}$  is the left eigenvector corresponding to  $\lambda_i$  and  $B_j$  is the j-th column of B. Using the Euclidean norm  $\|\cdot\|$ , we can therefore establish that the potential numeric value of  $|B_{i,j}|$  is restricted to the range  $0 \leq |\tilde{B}_{i,j}| \leq ||\phi_{l,i}|| ||B_j||$ . In the same way, the entries  $\tilde{C}_{i,k}$  for the k-th row are composed by  $C_k \phi_{r,i}$  and restricted to  $0 \le |C_{i,k}| \le ||\phi_{r,i}|| ||C_k||$ .

We use the modal state transformation and the just mentioned observations to discuss a boolean criterion for the controllability and the observability of selected eigenmodes TW **Sibliothek**, Die approbierte gedruckte Originalversion dieser Diplomarbeit ist an der TU Wien Bibliothek verfügbar werk knowledge hub The approved original version of this thesis is available in print at TU Wien Bibliothek.

in the next section. Following this, we employ the observation on  $\tilde{m{B}}$  and  $\tilde{m{C}}$  to discuss continuous measures for the degree of controllability and observability in Sections 2.2.4 and 2.2.5.

### 2.2.3 PBH-Test

Following the idea of the modal state transformation, we now discuss a powerful tool to investigate the controllability and observability of certain eigenvalues in linear timeinvariant systems called the Popov-Belevitch-Hautus test (PBH-test) or Hautus criterion. It states that an individual eigenvalue  $\lambda_i$  of the system matrix **A** is controllable if

$$rank([(\mathbf{A} - \lambda_i \mathbf{I}), \mathbf{B}]) = n \tag{2.13}$$

holds, where  $n = \text{size}(\boldsymbol{x})$ . In a similar way an individual eigenvalue  $\lambda_i$  is observable if

$$rank([(\mathbf{A} - \lambda_i \mathbf{I}); \mathbf{C}]) = n \tag{2.14}$$

holds [33, 34].

When looking closer at those criterions we see that  $(A - \lambda_i I)$  is rank deficient in exactly the direction of the eigenvector  $\phi_i$ , corresponding to the eigenvalue  $\lambda_i$ . Hence the only way the criterion can be fulfilled is by B or C having some component in the direction of the eigenvector  $\phi_i$ . Thus, the criterion only state non-controllability for the *i*-th mode if all columns of **B** are exactly orthogonal to  $\phi_i$  [35].

According to this, the PBH-test is casting these relations of controllability or observability into a boolean answer. But it does not give any hints on how well a certain **B**-matrix makes the eigenvalue  $\lambda_i$  of our system controllable, or how well a certain C-matrix makes  $\lambda_i$  observable respectively. In practice a B-matrix with entries only in minor important direction of  $\phi_i$  (hence relatively small entries in  $B_i$ , which corresponds to  $\phi_i$  and the rows of **B** being close to orthogonal, see Section 2.2.2), makes the PBH-test suggest controllability of this eigenvalue.

For this reason we introduce a method which gives a more nuanced measure of the controllability and observability of eigenmodes in the next section. Based on this method, we then also elaborate further on a systematic approach to construct input and output matrices for given degrees of freedom in the choice of access points for control inputs and output signal selection.

# 2.2.4 Geometric Controllability and Observability

In the previous section we already discussed that the direction of the column  $B_i$  compared to the direction of the eigenvector  $\phi_i$  lets us evaluate if the corresponding eigenvalue  $\lambda_i$  is actually controllable with the input  $u_i$ .

Similarly, the direction of the row vector  $C_k$ , compared to the direction of  $\phi_i$ , provides information about the observability of the eigenvalue  $\lambda_i$  by the output  $y_k$ .

This motivates an alternative definition of modal controllability and observability, which provides a more differentiating assessment compared to the PBH-Test. The so-called geometric controllability measure  $m_{\text{ctrb}}$  and geometric observability measure  $m_{\text{obsy}}$  are defined as

$$m_{\operatorname{ctrb},i,j} = \cos(\angle(\boldsymbol{\phi}_{l,i}, \boldsymbol{B}_j)) = \frac{\|\boldsymbol{\phi}_{l,i}^T \boldsymbol{B}_j\|}{\|\boldsymbol{\phi}_{l,i}\| \|\boldsymbol{B}_j\|}$$
(2.15)

and

$$m_{\text{obsv},i,k} = \cos(\angle(\boldsymbol{\phi}_{\text{r},i}, \boldsymbol{C}_k)) = \frac{\|\boldsymbol{C}_k \boldsymbol{\phi}_{\text{r},i}\|}{\|\boldsymbol{\phi}_{\text{r},i}\| \|\boldsymbol{C}_k\|}.$$
 (2.16)

In this definitions  $B_j$  is the j-th column of B,  $C_k$  is the k-th row of C and  $\phi_{l,i}$  and  $\phi_{\mathbf{r},i}$  are the left and right eigenvector corresponding to  $\lambda_i$ . For  $\boldsymbol{B}_i$  parallel to  $\phi_{\mathbf{l},i}$ this definition gives the maximum measure of controllability  $(m_{\text{ctrb},i,j}=1)$ , and with  $B_j$  orthogonal to  $\phi_{l,i}$  it gives the minimum measure  $(m_{\text{ctrb},i,j}=0)$ . The geometric observability measure  $m_{\text{obsv},i,k}$  works respectively [36, 37, 38].

This definition of controllability measures enables us to directly find the single most effective control input location to dampen the eigenvalues of the inter-area and in-area-1 oscillations.

Therefore, we select single input locations by setting the corresponding entry in  $B_{\text{test},i}$ to 1, whereas all others are set to 0. To find the most effective input from the generator unit G1, we can constrain the selection of the nonzero entry of  $B_{\text{test},i}$  to states of this unit. The maximum geometric controllability score is reached when the single nonzero entry corresponds to the most dominant eigenvector direction (largest entry in the eigenvector).

Table 2.7 shows the geometric controllability scores of feasible input configurations corresponding to states of the generator unit G1. The state 'G1/STG/Govenor/Speed Regulator/Relay' denotes the opening- or closing-speed of the valve controlling the steam flow into the steam turbines. 'G1/EXCITER/Main Regulator' corresponds to the excitation voltage for the rotor windings. The scores are evaluated for the inter-area, in-area-1 and in-area-2 oscillation mode.

At this point we also want to recall, that the geometric controllability is only investigated on the linearized power system model, where strict (nonlinear) limitations of some state variables are ignored. For the affected states, the geometric controllability measures can suggest a better modal controllability than actually available in the nonlinear system.

Geometric Controllability of Eigenmodes			
	Geometric Controllability Score		
	eigenvalue	eigenvalue	eigenvalue
States	-0.26 ± 4.04i	-2.23 ± 8.00i	-1.79 ± 7.85i
	(f = 0.64 Hz,	(f = 1.32 Hz,	(f = 1.28 Hz,
	ζ = 0.06)	ζ = 0.26)	ζ = 0.22)
G1/STG/Governor/Speed Regulator/Relay	4.92e-6	1.5191e-6	5.2544e-7
G1/EXCITER/Main Regulator	3.8089e-7	8.8732e-7	2.7064e-7

Table 2.7: Geometric controllability measures  $(0 \le m_{\rm ctrb} \le 1)$  of the most critical eigenvalues evaluated for inputs belonging to different states from the generator unit G1.

# 2.2.5 Participation Factor

In the previous section we evaluated the geometric controllability measure by allowing only one nonzero entry in  $B_{\text{test},i} = 1$  corresponding to a state of the generator unit G1. This lets us use this measure to find the single best suited input location to actuate on the eigenmode corresponding to  $\lambda_i$ .

However, the geometric observability measure does not let us directly evaluate a collective observability measure for a selection of feedback signals. We do want to have such an evaluation method in order to choose the most important feedback signals to provide a good observability of specific eigenmodes. Once we provide a good observability of an eigenmode through the feedback signals, our controller can then actuate on them. In this section we discuss a method, proposed in [39], to find such a reduced selection of feedback signals  $x_S \subset x$  to accurately map specific eigenmodes of interest to a controller. If we are able to find a comparable small selection of important feedback signals, this lets us drastically simplify the feedback structure.

The relevance of specific states to certain eigenmodes of the system can be expressed through, so-called, participation factors, [40, 29, 35]. Based on this factor, the authors compute reduced order models which accurately reproduce selected modes and determine the components of the original system which are most involved in those modes. It is assumed, that the states with relatively high involvement carry most of the relevant information about the eigenmodes under consideration. Therefore, those states are proposed to be used as feedback signals to actuate on those eigenmodes. Following this, we aim to select the states with the highest participation factors for the eigenmodes under consideration as feedback signals, so that the controller gets passed a maximum of information about the eigenmodes of interest with a minimum number of feedback

The participation factor for the eigenvalue  $\lambda_i$  is defined by the normalized left and right eigenvectors,  $\Phi_{\mathbf{r},i}$  and  $\Phi_{\mathbf{l},i}$  so that

$$\mathbf{\Phi}_{\mathbf{l},i}^T \mathbf{\Phi}_{\mathbf{r},j} = \begin{cases} 1, & \text{if } i = j \\ 0, & \text{otherwise.} \end{cases}$$
 (2.17)

Then the magnitude of the dimensionless participation factor

$$p_{i,k} = \phi_{l,i,k}\phi_{r,i,k}. \tag{2.18}$$

measures the relative participation of the state  $x_k$  in the eigenmode corresponding to  $\lambda_i$ [29, 40]. In [35], the authors show that this also corresponds to a combined measurement of the geometric controllability and observability from Section 2.2.4.

Table 2.8 shows the states with the 10 largest magnitude values of participation factors.

Appendix A links the used state names to the equations from Section 2.1.1 and the block diagrams from Section 2.1.2. We immediately notice that the rotor angle and speed deviations evaluate to highly important states for the eigenmodes under investigation. This corresponds well to the observations in [39], even-though the power system model investigated in this thesis uses very detailed models of the electrical machines and the auxiliary devices.

Based on the evaluation in Table 2.8, we naturally select feedback signals with a strong involvement in the critical eigenmodes. This ensures that the feedback carries as much information about those modes as possible to the controller. However, when assembling such a set of feedback signals we also want to consider a few other restrictions. For example, the feedback signals should actually be measurable in a real life application. Thus states, such as the electromagnetic flux states, might drop out of a possible selection. Furthermore, the authors in [37] conduct further considerations about the variation of the controllability and observability measurements over the course of changing operating conditions. Hence, one might also discard states from a feedback selection, which have a strong variation of their participation factors over changing operating conditions. Such variation analysis is left out in this thesis, as the feedback signal selection focuses more on practical considerations. This will be discussed more in detail later in this thesis.

Pariticipation Factor for Eigenvalue -0.26 $\pm$ 4.04i (f = 0.64 Hz, $\zeta$ = 0.06)		
Rank	Rank State Magnitude	
1	G4/SM/Mechanical model/Δω	0.1874
2	G4/SM/Mechanical model/Δδ	0.1809
3	G1/SM/Mechanical model/Δω	0.1678
4	G1/SM/Mechanical model/Δδ	0.1617
5	G3/SM/Mechanical model/Δω	0.1333
6	G3/SM/Mechanical model/Δδ	0.1253
7	G2/SM/Mechanical model/Δω	0.0506
8	G2/SM/Mechanical model/Δδ	0.0468
9	G4/STG/Govenor/Speed Regulator/Pos.	0.0043
10	G3/EXCITER/Low Pass Filter 1	0.0039

Pariticipation Factor for Eigenvalue -2.23 $\pm$ 8.00i (f = 1.32 Hz, $\zeta$ = 0.26)		
Rank	Rank State Magnitude	
1	G2/SM/Mechanical model/Δω	0.4615
2	G2/SM/Mechanical model/Δδ	0.2856
3	G1/SM/Mechanical model/Δδ	0.1797
4	G1/SM/Mechanical model/Δω	0.1778
5	G2/EXCITER/Low Pass Filter 1	0.0474
6	G3/SM/Mechanical model/Δω	0.0323
7	G3/SM/Mechanical model/Δδ	0.0209
8	G1/EXCITER/Low Pass Filter 1	0.0177
9	G2/STG/Govenor/Speed Regulator/Pos.	0.0039
10	G4/SM/Mechanical model/Δδ	0.0026

Pariticipation Factor for Eigenvalue -1.79 $\pm$ 7.85i (f = 1.28 Hz, $\zeta$ = 0.22)		
Rank State Magnitude		
1	G3/SM/Mechanical model/Δω	0.3578
2	G4/SM/Mechanical model/Δδ	0.2463
3	G4/SM/Mechanical model/Δω	0.2444
4	G3/SM/Mechanical model/Δδ	0.2251
5	G3/EXCITER/Low Pass Filter 1	0.0228
6	G2/SM/Mechanical model/Δω	0.0190
7	G1/SM/Mechanical model/Δδ	0.0114
8	G1/SM/Mechanical model/Δω	0.0113
9	G2/SM/Mechanical model/Δδ	0.0112
10	G4/EXCITER/Low Pass Filter 1	0.0104

Table 2.8: Ranked participation factors for the most critical eigenvalues. The tables show the states with the highest participation in the corresponding eigenmodes. For a more detailed description of the states, see Appendix A.



# Optimal Controller Design

# 2.3.1 Linear Quadratic Regulator

In this section we discuss how we can design a controller using an optimality principle which ensures stability of our system. For this, we address the so-called linear-quadratic regulator (LQR) and how it provides an optimal control strategy for a given cost function.

The linear-quadratic regulator is one of the most important results in the field of optimal control. It provides an algorithm to calculate a feedback controller gain which ensures to stabilize a linear, time-invariant system that is stabilizable. For a linear state space system to be stabilizable all of its uncontrollable eigenmodes have to be asymptotically stable.

The resulting LQR controller does not only provide a stabilization, but is the result of an optimization problem in the terms of minimizing a quadratic cost function of the form

$$J(x, u) = \int_0^\infty (\boldsymbol{x}^T \boldsymbol{Q} \boldsymbol{x} + \boldsymbol{u}^T \boldsymbol{R} \boldsymbol{u} + 2\boldsymbol{x}^T \boldsymbol{N} \boldsymbol{u}) dt$$
 (2.19)

[41]. In this cost function definition we distinguish three different parts. The first part,  $x^TQx$ , defines the cost created by states x deviating from their set points. These state deviations are weighted by the entries of the matrix Q. The second term of the cost function,  $u^T R u$ , penalizes excessive control inputs u, again weighted by the matrix R. The third part of the cost function,  $2x^TNu$ , penalizes certain combinations of inputs u and state deviations x by the weights defined in N. This third part of the cost function is only noted here for the sake of completeness, but was not used throughout the work for this thesis. Hence we set N = 0. Q and R have to be symmetric and positive definite [41, 42].

The solution of this optimization problem, defined with the cost function and the linear state space system, can be found by solving the so-called algebraic Riccati equation

$$A^{T}S + SA - (SB + N)R^{-1}(B^{T}S + N^{T}) + Q = 0$$
 (2.20)

for S [41]. In this equation, A, B are the corresponding matrices from the linear state space system to control, and Q, R, N are the weighting matrices from the cost function definition. The feedback gain K for a feedback control law in the form of u = -Kx is than derived from the solution of S by

$$\boldsymbol{K} = \boldsymbol{R}^{-1} (\boldsymbol{B}^T \boldsymbol{S} + \boldsymbol{N}^T) \tag{2.21}$$

[41]. The application of this control law then leads to the closed loop poles

$$P_{\rm cl} = \operatorname{eig}(\boldsymbol{A} - \boldsymbol{B}\boldsymbol{K}) \tag{2.22}$$

of the system, where eig() is the function evaluating the eigenvalues.

We already stated stabilizability of the linear system to be a main requirement for the LQR controller. However, we not only have to make sure that all uncontrollable eigenmodes are asymptotically stable, but we also have to make sure all unstable behavior causes increasing cost. For this reason Q is required to be positive semi-definite.

This can usually be achieved by assigning values larger than zero to the diagonal entries. In this case the resulting controller will put in more effort to bring higher weighted states to their reference values compared to states with smaller corresponding entries in the  $\boldsymbol{Q}$  matrix.

# 2.3.2 Modal Weighting Matrix

In the previous section we discussed how we can use the LQR method to design a controller and ensure a stable closed-loop behavior. We also briefly covered how the Q matrix of the quadratic cost function definition can emphasize or play down the importance of keeping state values close to their reference values. However, in this work we are not interested in emphasizing certain states to track a specific reference value. The controller we want to design shall dampen selected oscillation modes no matter what the actual current state values are. For applications like this, we can design the Q matrix for an LQR controller in a way that puts emphasis on combinations of states that correspond to the oscillation modes of interest.

To obtain such a weighting matrix  $\hat{Q}$ , we demand

$$\hat{\mathbf{Q}}\phi_k = \phi_k m_k \tag{2.23}$$

to be valid for a set of  $k = 1 \dots n$  open loop eigenvectors [42]. The scalar weights  $m_k$ assigned to each eigenvector are arranged in a diagonal matrix M, in the same way as the eigenvectors  $\phi_k$  are arranged into an eigenvector matrix  $\Phi$ . Then the preceding equation can be rewritten to

$$\hat{\mathbf{Q}} = \mathbf{\Phi} \mathbf{M} \mathbf{\Phi}^{-1}. \tag{2.24}$$

To make sure the Q matrix for the LQR algorithm is symmetrical we define

$$Q = \hat{Q}^T \hat{Q}. \tag{2.25}$$

If we plug this definition of Q into our quadratic cost function definition of the LQR algorithm from Eq. (2.19) and evaluate the cost for a state combination corresponding to a critical eigenvector  $s_k$ ,

$$\phi_k^T \mathbf{Q} \phi_k = \phi_k^T \hat{\mathbf{Q}}^T \hat{\mathbf{Q}} \phi_k = m_k^2 \text{ with } \operatorname{abs}(\phi_k) = 1$$
 (2.26)

we see that the weighting for a state combination of an unwanted oscillation mode is exactly the squared weight  $m_k^2$  assigned to that eigenvector.

This, of course, assumes full state feedback. In a subsequent section, we will further proceed to adapt this method for a controller which does not have full state feedback.

# 2.3.3 Linear Quadratic Regulator for Output Feedback

In the previous sections, we summed up the tools to design a modal damping LQR controller based on a full state feedback. In this section we will extend those tools to design a controller, based on the modal LQR approach, which needs only a subset of the states as feedback signals. This facilitates the controller implementation into real world applications, as many of the states of the simulation model are difficult to measure. For example the electromagnetic fluxes between the generator stator and rotor can hardly be measured directly to fit the definitions of the corresponding states in the simulation model. Additionally, some states react very quickly to disturbance events or control inputs, hence an effective utilization of such states would also require a very fast and robust communication network between the grid components.

To select the feedback signals from the state vector we define a signal selection matrix  $C_{\rm S}$ , according to an output matrix, so that the selected feedback states  $x_{\rm S}$  are

$$x_{\rm S} = C_{\rm S} x$$
 for  $x$  from  $\dot{x} = Ax + Bu$ . (2.27)

We notice that  $x_{\rm S}$  is defined in an analogous way to an output definition y = Cx. This allows us to use a so-called output feedback controller design approach to define a control law based on  $x_{\rm S}$ . In the following, we show the design of an optimal controller based on selected feedback states  $x_{\rm S}$ . Thereby, we use the same optimality principle as for the full state feedback LQR. Subsequently, we will briefly discuss how to select feedback signals to design an effective modal damping controller.

To elaborate the changes for the optimization problem of our output feedback controller, we compare the output feedback to the full state feedback structure. We immediately recognize some differences in the control law and the closed-loop dynamics. The original control law u = -Kx of the full state feedback becomes

$$u = -Ky = -KCx$$
 or  $u = -Kx_S = -KC_Sx$  (2.28)

for the output feedback and the feedback of selected states respectively.

Consequently, when applying the control law from Eq. (2.28), the closed-loop dynamics change from

$$\dot{\boldsymbol{x}} = \boldsymbol{A}\boldsymbol{x} - \boldsymbol{B}\boldsymbol{K}\boldsymbol{x} \tag{2.29}$$

for the full state feedback, to

$$\dot{x} = Ax - BKCx$$
 respectively  $\dot{x} = Ax - BKC_Sx = A_Cx$ . (2.30)

Plugging the control law with the selected states as output feedback from Eq. (2.28) into the cost function definition Eq. (2.19) (omitting the cross-weighting term, hence N=0), we can come up with a symmetric matrix P, so that

$$\frac{d}{dt}(\boldsymbol{x}^{T}\boldsymbol{P}\boldsymbol{x}) = -\boldsymbol{x}^{T}(\boldsymbol{Q} + \boldsymbol{C}_{S}^{T}\boldsymbol{K}^{T}\boldsymbol{R}\boldsymbol{K}\boldsymbol{C}_{S})\boldsymbol{x}$$

$$= \dot{\boldsymbol{x}}^{T}\boldsymbol{P}\boldsymbol{x} + \boldsymbol{x}^{T}\boldsymbol{P}\dot{\boldsymbol{x}} = \boldsymbol{x}^{T}(\boldsymbol{A}_{S}^{T}\boldsymbol{P} + \boldsymbol{P}\boldsymbol{A}_{S})\boldsymbol{x}.$$
(2.31)

If we can actually find such a constant, positive semi-definite matrix P, this definition converts the dynamical optimization problem into an equivalent static problem [43]. For this to hold true for all initial condition and all trajectories, where we expect the cost to always vanish for  $t \to \infty$ , we can rearrange Eq. (2.31) and, for a given K, solve the resulting equation

$$0 = \boldsymbol{A}_{\mathrm{C}}^{T} \boldsymbol{P} + \boldsymbol{P} \boldsymbol{A}_{\mathrm{C}} + \boldsymbol{C}_{\mathrm{S}}^{T} \boldsymbol{K}^{T} \boldsymbol{R} \boldsymbol{K} \boldsymbol{C}_{\mathrm{S}} + \boldsymbol{Q}$$
 (2.32)

for P, which is closely related to the algebraic Riccati equation 2.20 [44]. Since we do not know K, but want to find its optimal entries, this leads us to an iterative procedure to find the optimal controller gain K. Throughout this iterative procedure, Eq. (2.32)then ensures that the boundaries given by the system dynamics are fulfilled.

In practice however, the iterative approach to elaborate such an output feedback gain often reaches its limits very soon. [44] therefore proposes necessary and sufficient conditions for convergence of the controller gain optimization. Having said this, many of the iterative methods proposed in [43, 45, 44] only work sufficiently well on small systems, but fail to converge or struggle with numerical issues on larger systems (such as algorithm 1 from [44] on our current linearized power grid system). To overcome these issues, [46] and [44] propose specialized optimization algorithms. For the results proposed in this thesis, we used algorithm 2 from [44] with a slightly relaxed stopping criterion (stopCrit = 1e - 6).

Finally, we have to elaborate on the selection of feedback signals for the output feedback LQR controller. As already mentioned above, measurements of the state signals shall be accessible in reality. Furthermore, in order to actively dampen certain oscillation modes, we have to recognize those critical oscillations through the feedback signals. Hence the feedback signals shall collectively provide good information about the oscillation modes to dampen. For this reason, we select feedback signals which have a high participation in the modes of interest, see Section 2.2.5. The set of feedback states is selected via the aforementioned signal selection matrix  $C_{\rm S}$ . The output feedback LQR controller gain is then calculated with the system matrices  $A, B, C_{\rm S}$  and the modal weighting Q-matrix from Section 2.3.2.

The resulting controller will usually have a less precise influence on the targeted system poles then a full state feedback controller. Hence it is also going to shift poles which are not weighted in the modal weighting Q-matrix. One way to avoid this drawback is to develop an observer, which calculates an estimation of the full state feedback based on the selected feedback signals. However, such an observer has to be carefully designed and tuned by its own, using knowledge of the underlying system. In the case of this work, we considered the development of an observer to introduce to much design effort not related to the critical eigenmodes under consideration.

# 2.3.4 Setpoint Tracking

Although we already stated that the controller to be designed should not track any specific reference setpoint, but shall react only on specific state combinations, we do not achieve this by a constant state feedback controller gain. The modal LQR feedback controller gain will still generate a control input if the system is in a steady state other than the one used for the design.

However, the power grid system under consideration in this work is able to operate at different steady state operating points. They might be reached by a different distribution of power inputs between the four generators. Or they might be reached by a concurring increase or decrease of power consumption and inputs. Additionally we have to consider that the controller actuating only on states of the generator unit G1 does not have full state controllability with respect to the whole power grid system. Therefore, it is simply not possible for our controller to steer the system back to its original operating point after any disturbance event. As a consequence the controller has to cope with the external conditions of the power grid operation after an event, even though the feedback states might not exactly correspond to the values anticipated by the controller gain for steady state operation. Knowing that the controller will be trying to restore original state values after any disturbance but will be unable to do so, we want to avoid any unnecessary control inputs. For this reason the controller actuation shall become zero as soon as the critical oscillations are sufficiently dampened.

We achieve this behavior by adding a fade-out on the controller actuation. The controller is thus able to apply its full potential of control actuation for a short period after an event. But after this initial period the further controller actuation is progressively scaled down to zero. Until a recurrence of the critical oscillations modes in the feedback signals is registered and the controller can use its full actuation potential again. In the case of our controller, which is directly acting on the excitation voltage and therefore influences the terminal voltage of the generator, the fade-out of the control input is actually critical to reach the reference terminal voltage of the generator after a disturbance event. This is important to keep the grid voltage on its required level. For the exact same reason the original PSS is also equipped with a wash-out transfer

function, see Section 2.1.2 and Fig. 2.6. At this point, we want to re-interpret this wash-out transfer function not as an adhoc solution to avoid a steady controller actuation, but as a variation of the idea of

the integration of the control error. When adding an integration of the control error to a feedback loop, we add an additional system state to make sure any deviation of the closed-loop output to the output reference due to modeling inaccuracies or system

disturbances will asymptotically become zero.

In the present case of the damping controller, we do not care about any specific output

reference, but we only want the control output to asymptotically become zero after any disturbance. This means, we do not want to react to a persistent difference between the output and the output reference, but we want to avoid a persistent difference between the control input to our system and an, always zero, reference control input. If those signals deviate for a certain duration, hence the integral of their difference becomes notable, we want to correct for that. When transforming this integrating control input feedback loop, illustrated in Fig. 2.11, we end up with the same transfer function, as with an additional wash-out transfer function.

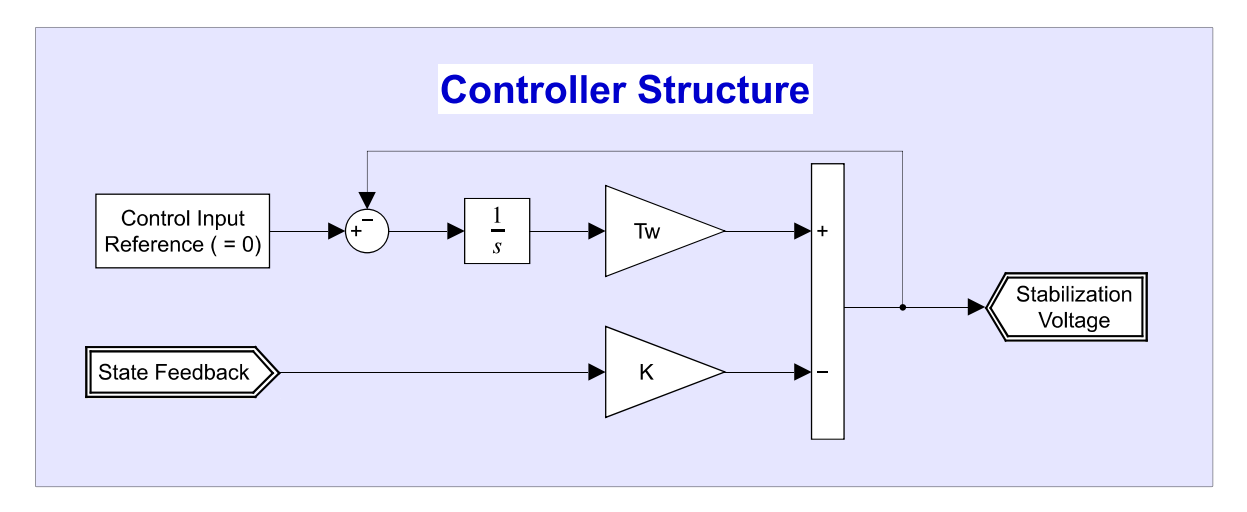


Figure 2.11: Block diagram of the LQR controller with the setpoint integration. The gain K is the LQR controller feedback gain and the gain  $T_{\rm w}$  is a manually tuned time constant of the wash-out/setpoint integration and is set to  $T_{\rm w}=0.5$  for all simulation runs presented in this thesis.

The controller output  $V_{\text{stab}}$  expressed by the state vector  $\boldsymbol{x}$  gives

$$V_{\text{stab}} = -\mathbf{K}\mathbf{x} + (0 - \frac{V_{\text{stab}}}{T_{\text{w}}}s)$$

$$\Rightarrow V_{\text{stab}} = \frac{-\mathbf{K}\mathbf{x}}{(1 + \frac{1}{T_{\text{w}}}s)} = -\mathbf{K}\mathbf{x}\frac{T_{\text{w}}s}{(T_{\text{w}}s + 1)}$$
(2.33)

with the controller gain K and a tunable time constant for the wash-out  $T_{\rm w}$ . The transfer function of the wash-out  $G_{\text{washout}}$  is defined as

$$G_{\text{washout}} = \frac{T_{\text{w}}s}{(T_{\text{w}}s+1)}.$$
(2.34)

Using the expression for  $V_{\text{stab}}$  to obtain the controller transfer function yields

$$G_{\text{controller}} = \frac{V_{\text{stab}}}{x} = -K \frac{T_{\text{w}}s}{(T_{\text{w}}s+1)} \equiv -KG_{\text{washout}}.$$
 (2.35)

This can also be interpreted as adjusting the reference setpoint of the system to disturbances, so they do not cause constant control inputs. The time constant for the setpoint integration (or wash-out) can be tuned manually. For all simulation results we present in this thesis, we set  $T_{\rm w}=0.5$  which was chosen in reference to the original configuration with the PSS device.

If we do not want to tune this time constant manually, we can use the LQR method from Section 2.3.1 or Section 2.3.3 to optimize it simultaneously with the controller gain. In that case we introduce the additional state variable

$$p(t) = \int_{0}^{t} (u_{\text{ref}}(\tau) - u(\tau))d\tau$$
 (2.36)

which corresponds to the output of the integrator block in Fig. 2.11. With Eq. (2.36) and  $u_{\rm ref}(\tau) = 0$ , we then augment the state space system of the power grid and obtain

$$\begin{bmatrix} \dot{\boldsymbol{x}} \\ \dot{p} \end{bmatrix} = \underbrace{\begin{bmatrix} \boldsymbol{A} & \mathbf{0} \\ \mathbf{0} & 0 \end{bmatrix}}_{\boldsymbol{A}_{\text{aug}}} \underbrace{\begin{bmatrix} \boldsymbol{x} \\ p \end{bmatrix}}_{\boldsymbol{x}_{\text{aug}}} + \underbrace{\begin{bmatrix} \boldsymbol{B} \\ -1 \end{bmatrix}}_{\boldsymbol{B}_{\text{aug}}} \boldsymbol{u}. \tag{2.37}$$

Likewise we augment the weighting matrix

$$\mathbf{Q}_{\text{aug}} = \begin{bmatrix} \mathbf{Q} & \mathbf{0} \\ \mathbf{0} & m_{\text{w}} \end{bmatrix} \tag{2.38}$$

where Q is the modal weighting matrix from Section 2.3.2 and  $m_{\rm w}$  is an additional weighting factor for the integration of the control input. From the LQR method we then obtain the optimized controller gain  $K_{\text{aug}} = |K| T_{\text{w}}|$ .

However, in the case of this thesis we chose the manual tuning of the controller wash-out to avoid the additional complexity of simultaneously tuning the weighting Q and  $m_{\rm w}$ and to ensure a similar behavior compared to the original configuration with the PSS device.

# Chapter 3

# Results

# 3.1 Full State Feedback

In this chapter we discuss how the previously mentioned methods have been used to design different controller configurations for damping inter-area and in-area-1 oscillations. We present the results obtained from linear analysis during the design process and simulation results from the nonlinear Simulink model of the Kundur-2-Area System. All of the controller designs assume direct measurement of model states within the limits mentioned in Section 2.1.6. The first controller we will present assumes all model states are available as such measurement. This is less of a feasible assumption for controllers actually applicable in reality, but will serve as a benchmark in comparisons with the following controller designs. Those following controllers are designed based on feedback signals, which are restricted to a small selection of model states. The selection of feedback signals follows the treatise from Section 2.2.5, and shall provide a more realistically realizable approach.

However, all controller designs have in common that the controller output is only the stabilization voltage for the generator unit G1. All other generator units (G2-G4) stay untouched compared to the original grid configuration described in Section 2.1. The results are compared to simulation runs with the original grid configuration and a classical PSS device installed in generator unit G1(denoted with PSS in the plots). Furthermore the applied controllers are all equipped with the wash-out described in Section 2.3.4. The controller gains are designed with the methods from Sections 2.3.1 and 2.3.2 for the full state feedback benchmark and with the method from Section 2.3.3 for the controller with only selected feedback signals. The weighting decisions will be discussed in the following, but in general we adapted only the weighting factors of the inter-area and in-area-1 oscillation modes. All other eigenmodes of the system remained unweighted.

The linear state space system of the power grid is obtained directly from the Simulink



model using the 'Model Linearizer App' and the similarity transformation from Section 2.1.6.

When adjusting the weights for the inter-area and in-area-1 modes we generally paid attention to not overly strong influence poles other than the ones under consideration. With the assumption of full state feedback, we could not observe any unwanted influence on other poles. However this criterion becomes more important when using only a subset of the states as feedback signals.

Furthermore, we wanted to put more emphasis on damping the inter-area oscillation but still hinder extensive in-area-1 oscillations. But since the methods from Section 2.2.4 show that, with the given controller, we have a much higher controllability of the in-area-1 mode than of the inter-area mode, the in-area-1 mode requires significantly smaller weights compared to the inter-area mode.

Finally we also have to consider the physical limitations of certain grid components, when tuning the controller gain indirectly via the modal weights. As described in Section 2.1.2 the original PSS and the exciter model have limitations of their output voltages. Excessively exceeding those limitations would impair the performance of the controller. Therefore, we want to make sure the controller output, the stabilization voltage, complies to the original limits of the PSS output, and the excitation voltage also does not run into the given limits. This basically means the modal weights must not be chosen overly large.

Carefully balancing those criteria lets us decide on the weights shown in Table 3.1 and results in the controller gain specified in Tables 3.2 and 3.3. The state names used in those tables are linked to the equations discussed in Section 2.1.1 and the block diagrams from Section 2.1.2 in Appendix A. The modification of the system poles due to the application of the controller gain is visualized in Fig. 3.1. We can see, that the controller application moves the system poles of the inter-area oscillation to a much more damped location. Also the poles of the in-area-1 and in-area-2 oscillations are moved to a slightly more damped location, whereas all other system poles stay at their initial location.

In Fig. 3.2 and Fig. 3.3 we can see the results of the loadstep simulations with the nonlinear Simulink grid model and the full state feedback modal LQR the controller deployed in G1. Figure 3.2 shows the simulation results for a loadstep in Load 1, whereas Fig. 3.3 shows the simulation results for the event at Load 2.

The frequency dip of the generator frequencies after the loadstep of Load 1 is even less deep than with the original PSS configuration. Whereas after the loadstep of Load 2 the minimal frequency slightly exceeds the one with the original PSS configuration. In general the maximal frequency deviation after a disturbance event is an important criterion in terms of the frequency stability of the power system [4].

Nevertheless, the proposed controller, although it is only deployed in the generator

ie approbierte gedruckte Originalvers	The approved original version of this th
Die approbierte	The approved
oliothek	nowledge hub

Eigenvalue Weighting for Modal Weighting Matrix			
Weights			
Eigenvalue	full state	Δδ + Δω	Δω
	feedback	feedback	feedback
-0.26 ± 4.04i (f = 0.64 Hz, ζ = 0.06)	0.15	0.15	0.5
-2.23 ± 8.00i (f = 1.32 Hz, ζ = 0.26)	0.003	0.012	0.0005
-1.79 ± 7.85i (f = 1.28 Hz, ζ = 0.22)	0.06	0	0

Table 3.1: Summary of all the weighting factors for eigenvalues used to generate the modal damping Q-matrix for the LQR controller.

unit G1, is able to dampen the generator frequency oscillations very effectively. Approximately 2 seconds after the loadstep event, either through Load 1 or Load 2, we cannot observe any significant oscillations any more. This is a very good improvement compared to the original configuration.

Throughout the Simulink simulation runs, we also record the measurements of active and reactive power transfer over the inter-area lines, see Fig. 2.1. The resulting measurements for steps of Load 1 and Load 2 are plotted in Fig. 3.4.

As we can see in those measurements, the controller in G1 does not only reduce the frequency oscillation, but, with that, also reduces the peak loads of the inter-area power lines. This is especially noticeable for the apparent power S. Since the apparent power is defined by the active power P and the reactive power Q as

$$S = \sqrt{P^2 + Q^2},\tag{3.1}$$

it is an important measurement for the dimensioning of power lines. The reduction of peak apparent power transfer is particularly prominent after the increase of Load 2.

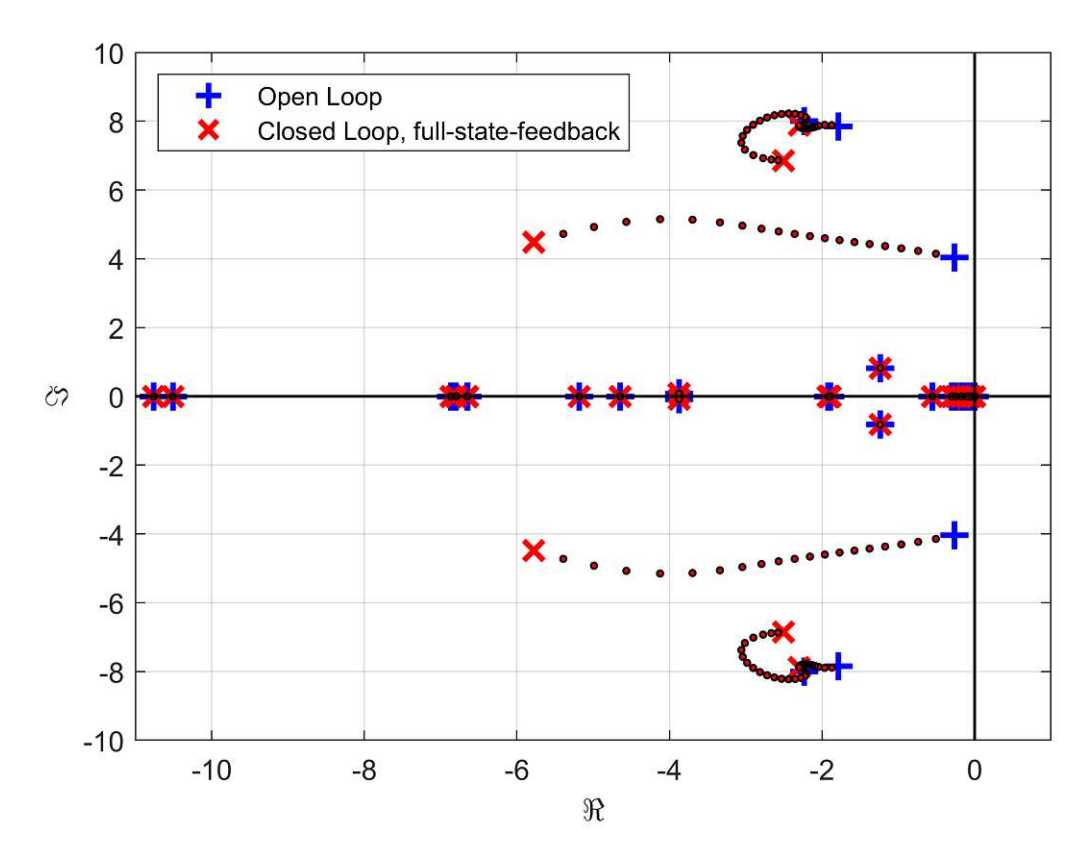


Figure 3.1: Eigenvalues of the linearized power grid system without the LQR controller ('Open Loop') and with the full-state-feedback LQR controller in place ('Closed Loop').

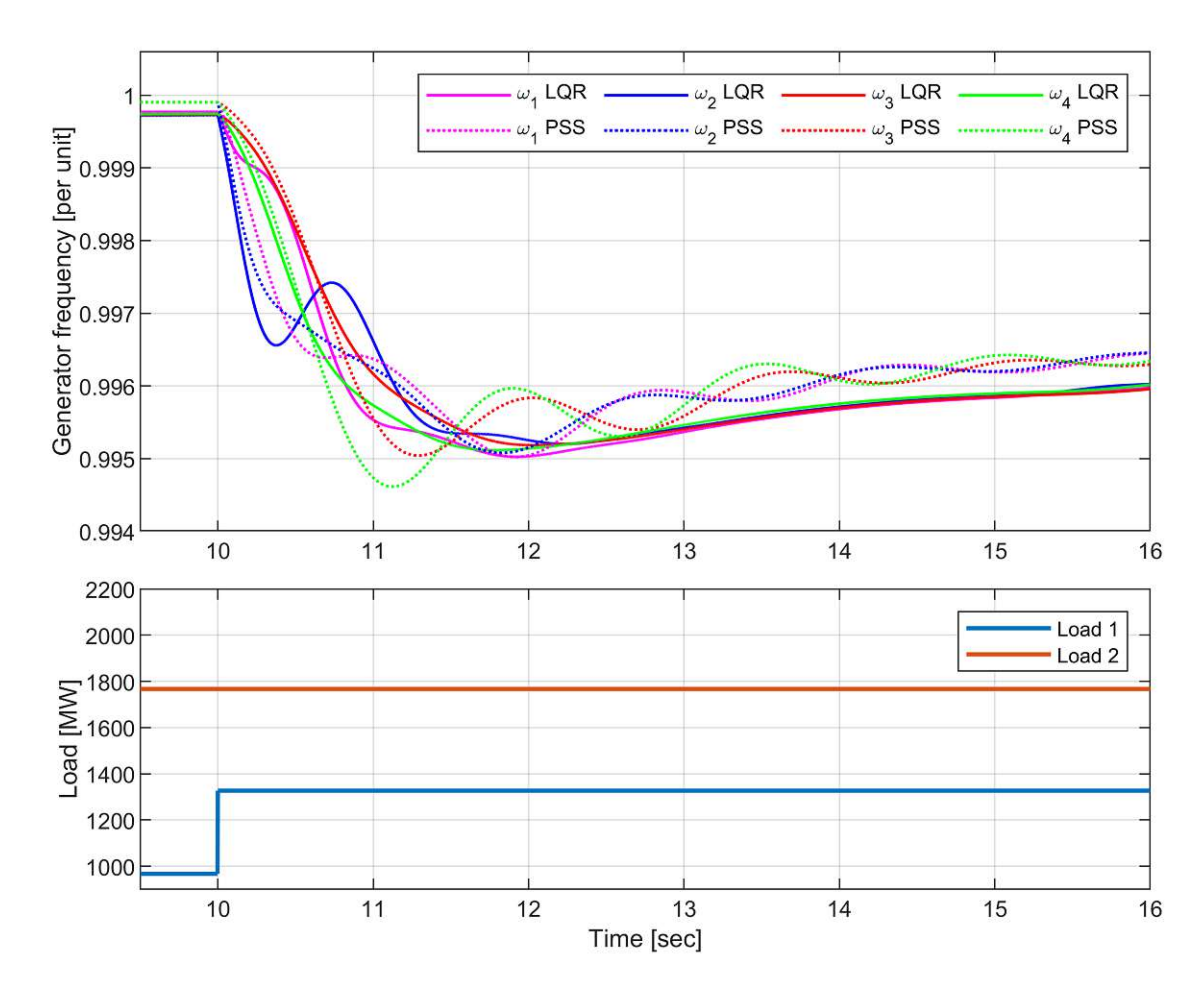


Figure 3.2: Simulink simulation results of a loadstep at Load 1 with the fullstate-feedback LQR controller acting on the stabilization voltage of the generator unit G1.

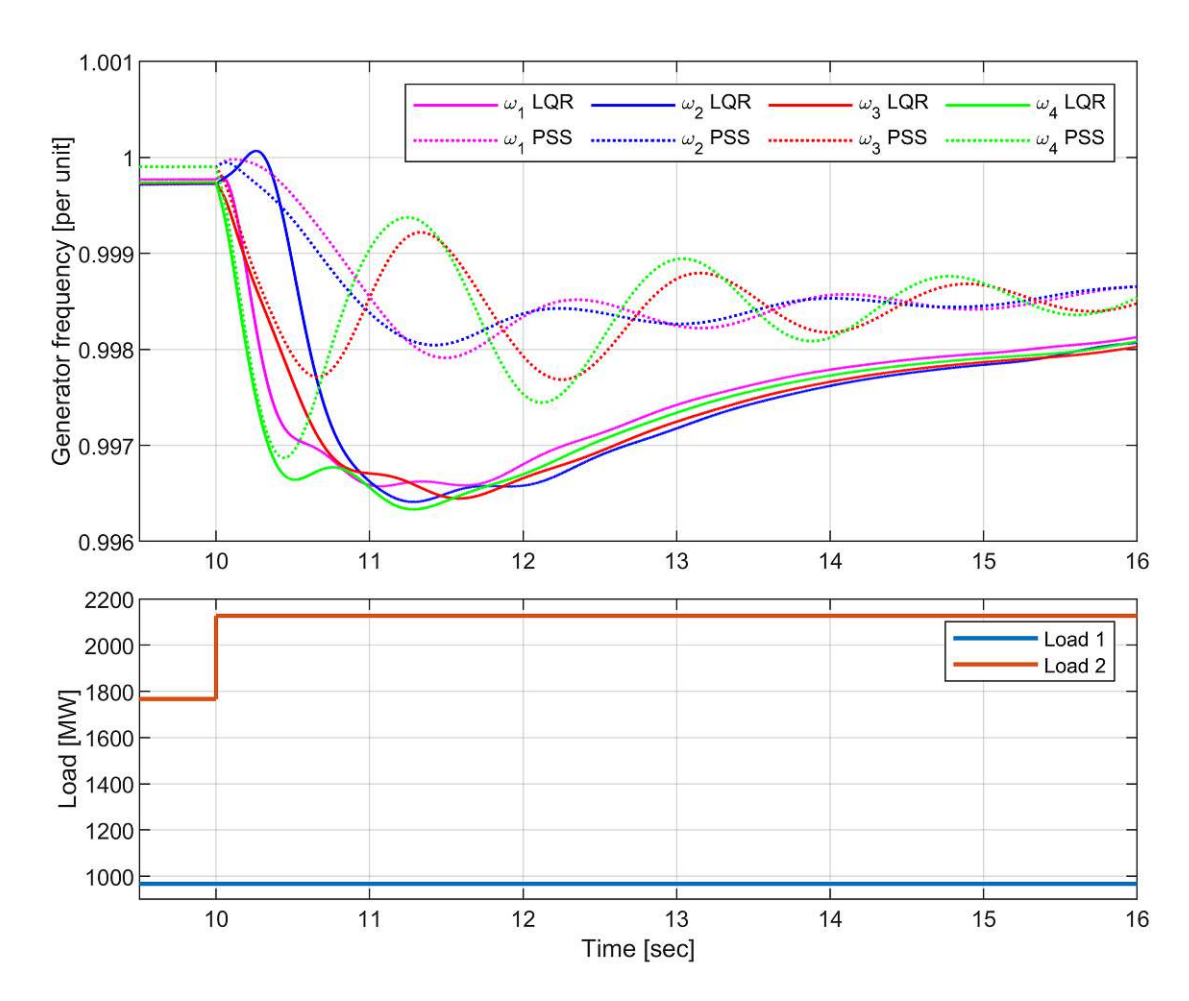


Figure 3.3: Simulink simulation results of a loadstep at Load 2 with the fullstate-feedback LQR controller acting on the stabilization voltage of the generator unit G1.

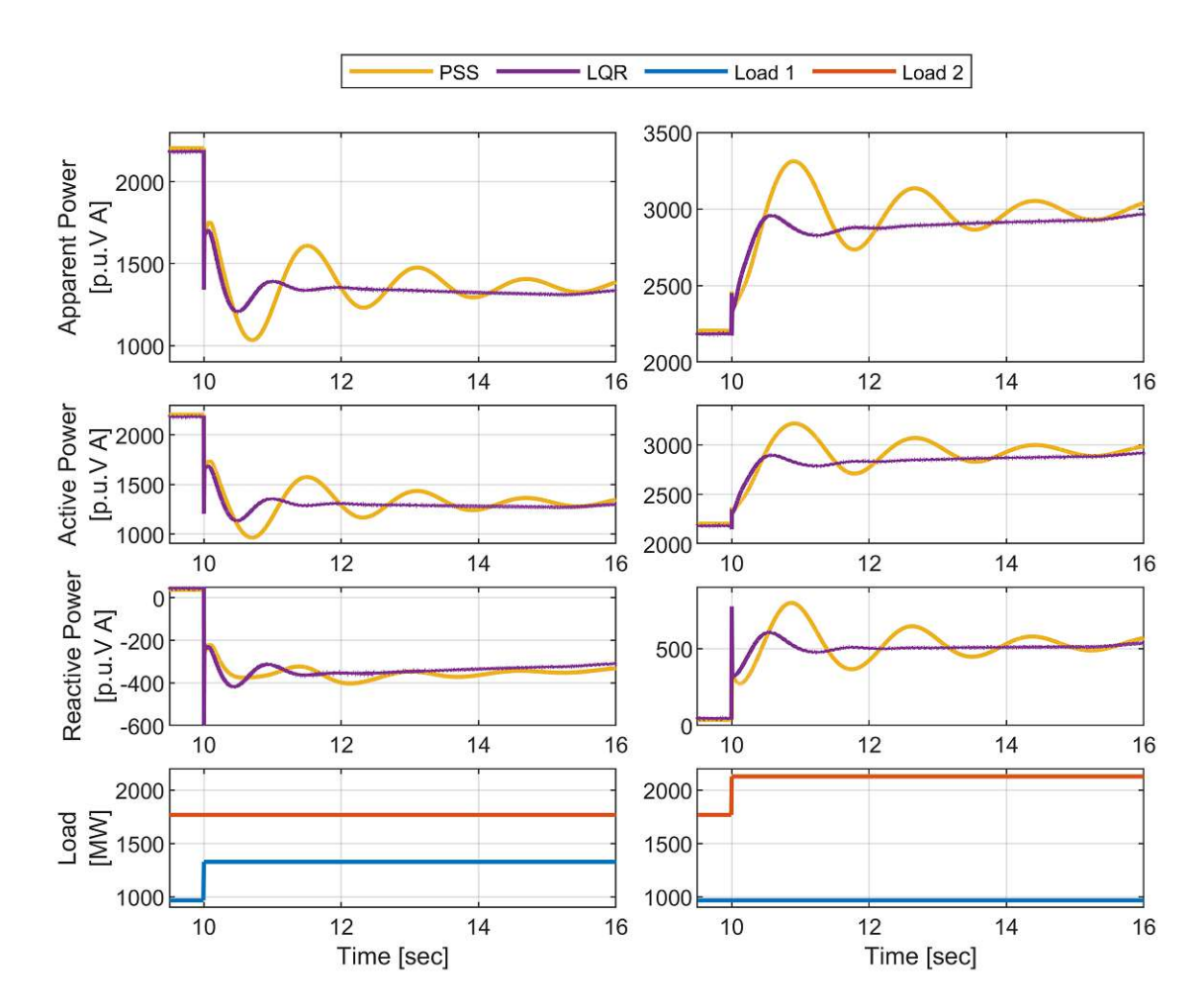


Figure 3.4: Inter-area power transfer from Simulink simulation runs with loadsteps at either Load 1 or Load 2 and the full-state-feedback LQR controller installed in generator unit G1.

# 3.2 Reduced Set State Feedback

After presenting the benchmark modal damping LQR controller with full state feedback in the last section, we subsequently present two modal damping LQR controllers which use only subsets, or reduced sets, of states as feedback. We present again simulation results of our power grid example with the proposed controllers applied.

The first step to design such a reduced set modal damping LQR controller, is to select the subset with the methods from Section 2.2.5. This follows the general idea, that the controller must receive adequate information about an oscillation mode in order to successfully act on it. The resulting ratings of feedback signals is presented in Table 2.8. We notice that different feedback states are important for the observability of different modes. Because we want to consider the inter-area and the in-area-1 oscillation mode, we therefore have to manually select a compromise. Furthermore, we do not want to restrict our selection of feedback signals to a certain configuration of the power grid, but rather find a subset as general as possible. Following this, we restrict our selection to choose the same signals from every generator. Through all those considerations we consider only the rotor speed and angle deviation signals as possible feedback signals. Some other states from the exciter model or the PSS device might be ranked more beneficial, but when replacing, for example, one of the generator units by a power converter, those states would not exist for this device any more. However, the rotor speed or angle deviation signal correspond to the frequency or phase deviation of a power converter.

To design the reduced set of modal damping LQR controller gains  $K_{\Delta\delta+\Delta\omega}$  and  $K_{\Delta\omega}$ , we use the method introduced in Section 2.3.3. When comparing the resulting controller gains  $K_{\Delta\delta+\Delta\omega}$  and  $K_{\Delta\omega}$  to the full state feedback controller gain  $K_x$ , we have to consider that they generate different controller outputs on the same scenarios when they are derived from the same weighting matrix Q. For this reason, we re-tuned the weighting matrix Q for the reduced set feedback controller. This re-tuning allows us to take full advantage of the original range of controller output limits and achieve similar performance with the reduced set feedback controllers. The selected weights and the resulting controller gains are specified in Table 3.1 and Tables 3.2 and 3.3 respectively. For a description of the used state names we again refer to Appendix A.

In Fig. 3.5 we compare the polemotion plots of the different feedback signal configurations. We observe that the controllers with reduced sets of feedback signals additionally influence poles other than the actually anticipated ones. However none of the unintentionally moved poles is becoming an additional critical oscillation mode. Although the rotor-speed-deviation-feedback configuration does unintentionally move one pole pair aggressively towards the right halfplane, a sufficient margin to the imaginary axis can be kept.

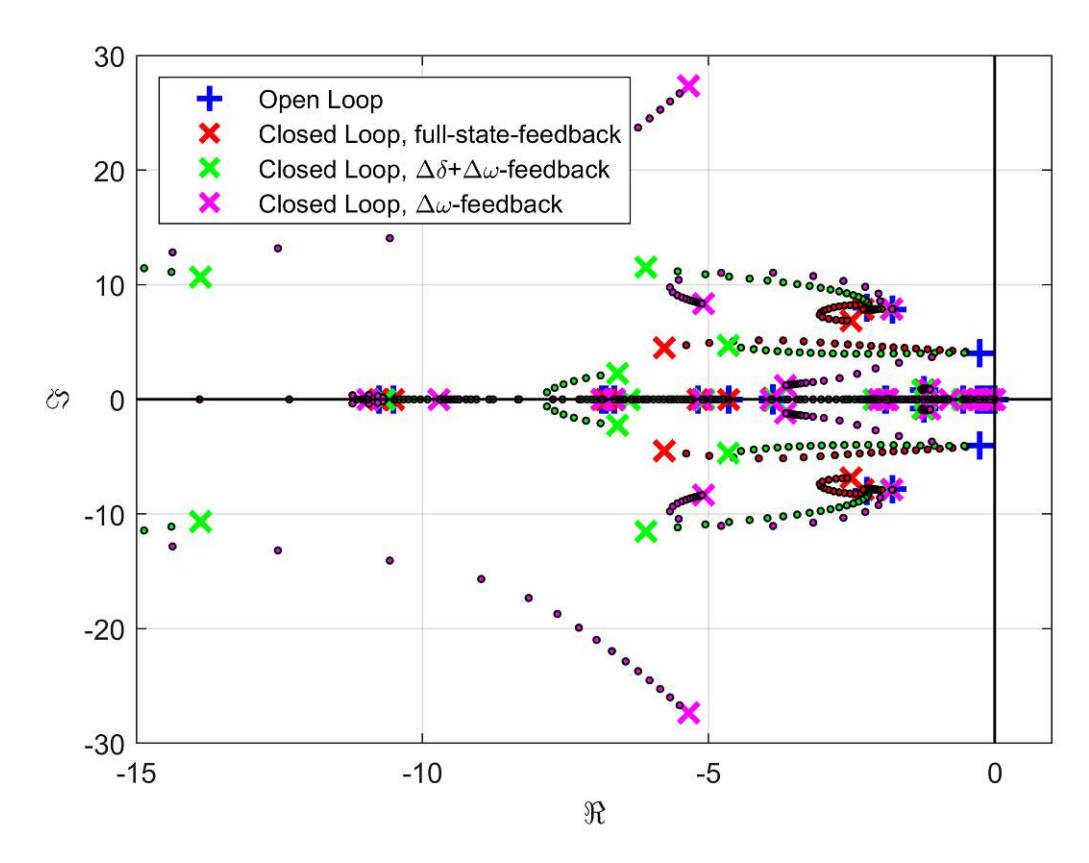


Figure 3.5: Eigenvalues of the linearized power grid system without the LQR controller ('Open Loop') and with a comparison of the different LQR controller configurations in place ('Closed Loop').

Figure 3.6, Fig. 3.7, Fig. 3.9 and Fig. 3.10 show the results of loadstep simulations with the two proposed reduced set feedback modal damping controllers deployed in G1. Figure 3.6 and Fig. 3.9 show the results of an increase in Load 1, whereas Fig. 3.7 and Fig. 3.10 show the results to the event in Load 2 respectively.

As described in Section 3.1, throughout the simulations the proposed controllers are only deployed in the generator unit G1. The rest of the power grid stays unchanged compared to the comparative example (denoted with PSS).

We can see that in all scenarios the proposed controllers are able to effectively dampen any generator frequency oscillation within less than 2 seconds after the loadstep event. The main difference compared to the simulation results in Fig. 3.2 can be observed in the behavior of the rotor speed of generator unit G1 shortly after the loadstep event at Load 1. Whereas with the full state feedback the graphs show only a slight bow to the right, this graph feature becomes much more prominent with the reduced set

feedback controllers. The controller with only rotor speed deviation feedback signals even slightly increases the rotor speed of generator unit G1 for a short time, before dropping like the other generator units (Fig. 3.9).

The fact that such an aggressive maneuver is necessary to keep the frequency dip close to the comparative configurations might already indicate a significant loss of sensibility through the reduction of feedback signals.

We also recorded the active and reactive power transfer over the inter-area power lines for the reduced set feedback controller configurations. Figure 3.8 shows the measurement for the controller with rotor angle and speed deviation feedback, and Fig. 3.11 shows the measurement for the controller with rotor speed deviation feedback only. Each plot shows the measurement after an event at Load 1 and Load 2 respectively.

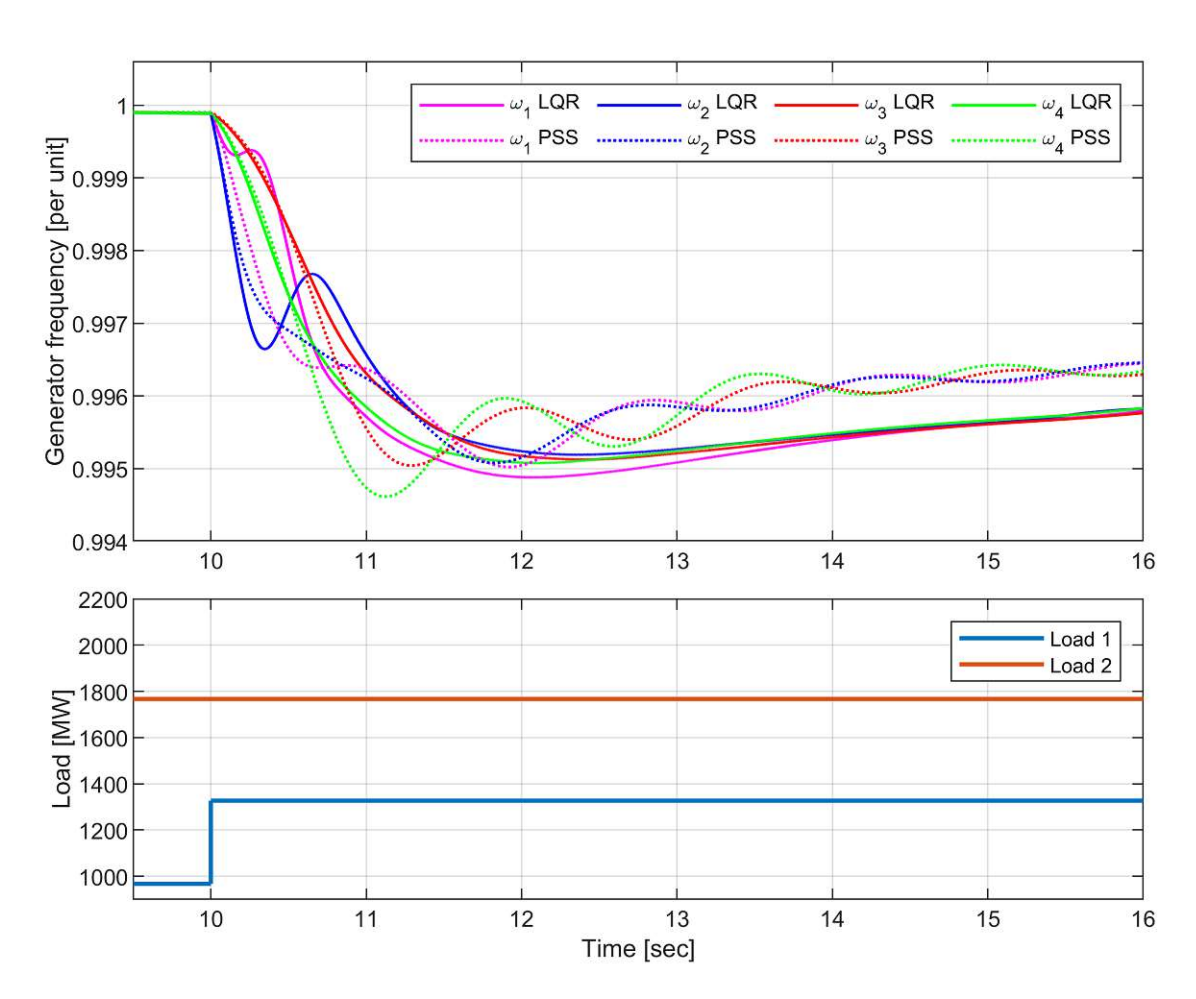


Figure 3.6: Simulink simulation results of a loadstep at Load 1 with the  $\Delta\delta$  +  $\Delta\omega$ -feedback LQR controller acting on the stabilization voltage of the generator unit G1.

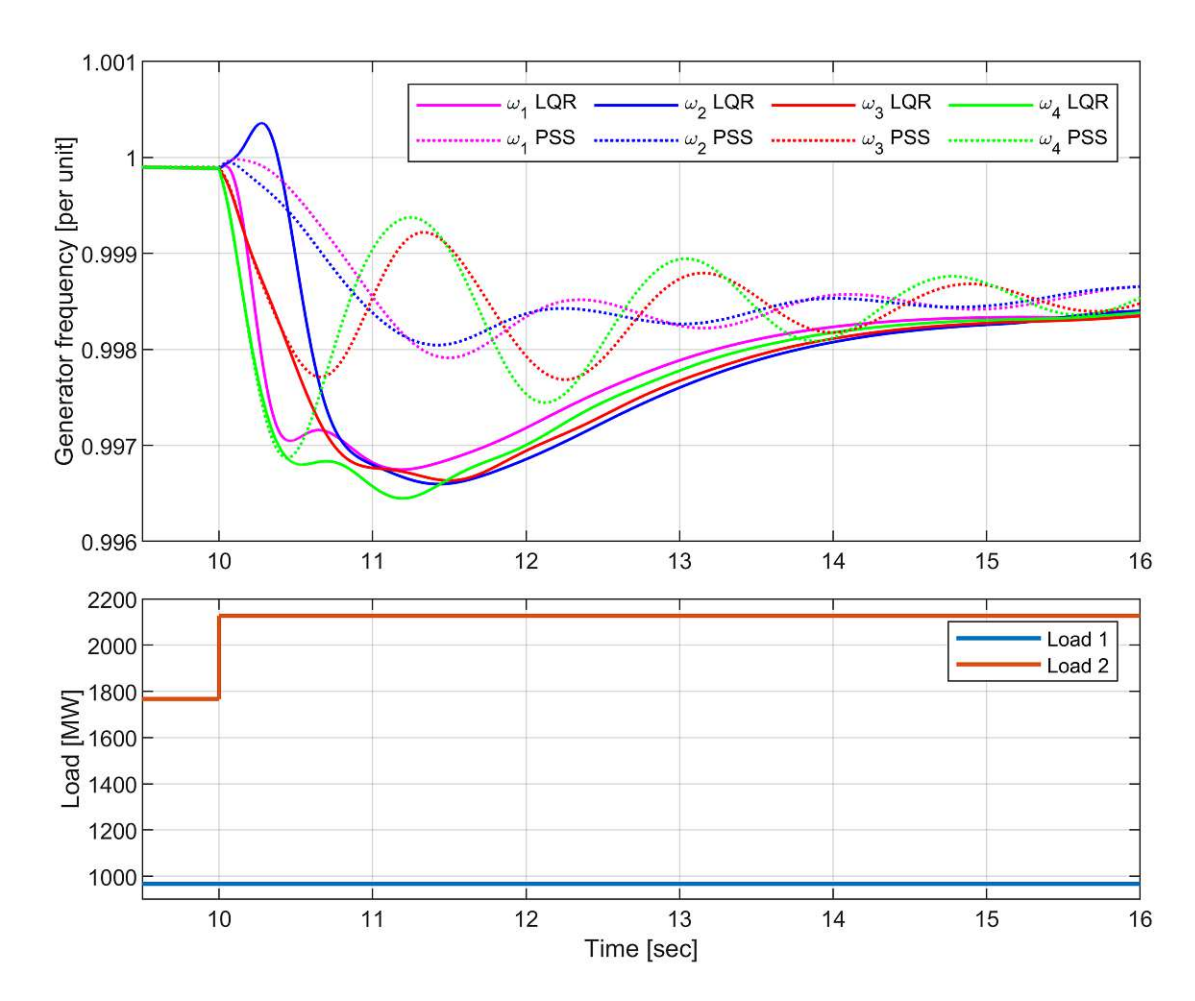


Figure 3.7: Simulink simulation results of a loadstep at Load 2 with the  $\Delta\delta$  +  $\Delta\omega$ -feedback LQR controller acting on the stabilization voltage of the generator unit G1.

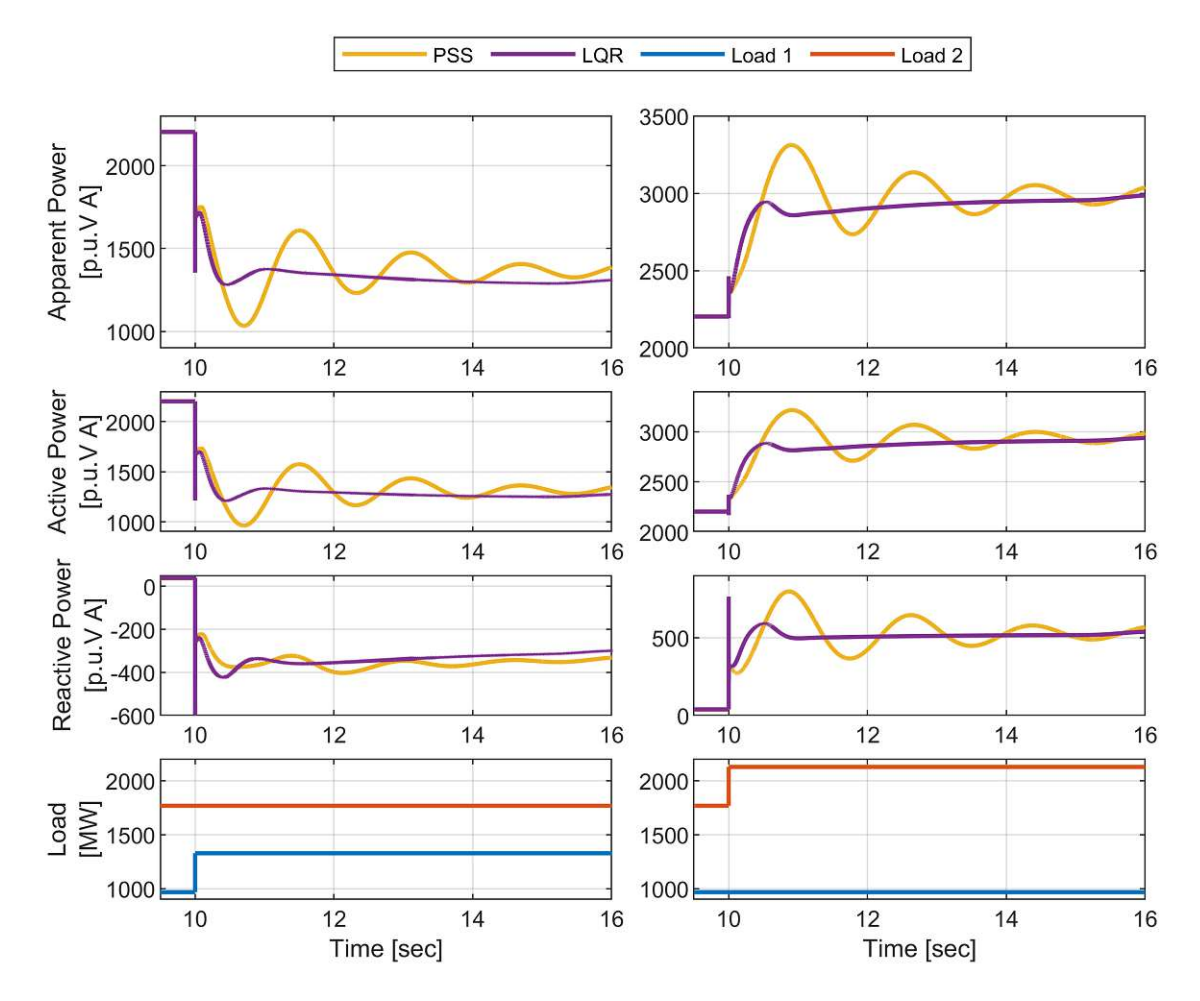


Figure 3.8: Inter-area power transfer from Simulink simulation runs with loadsteps at either Load 1 or Load 2 and the  $\Delta\delta + \Delta\omega$ -feedback LQR controller installed in generator unit G1.

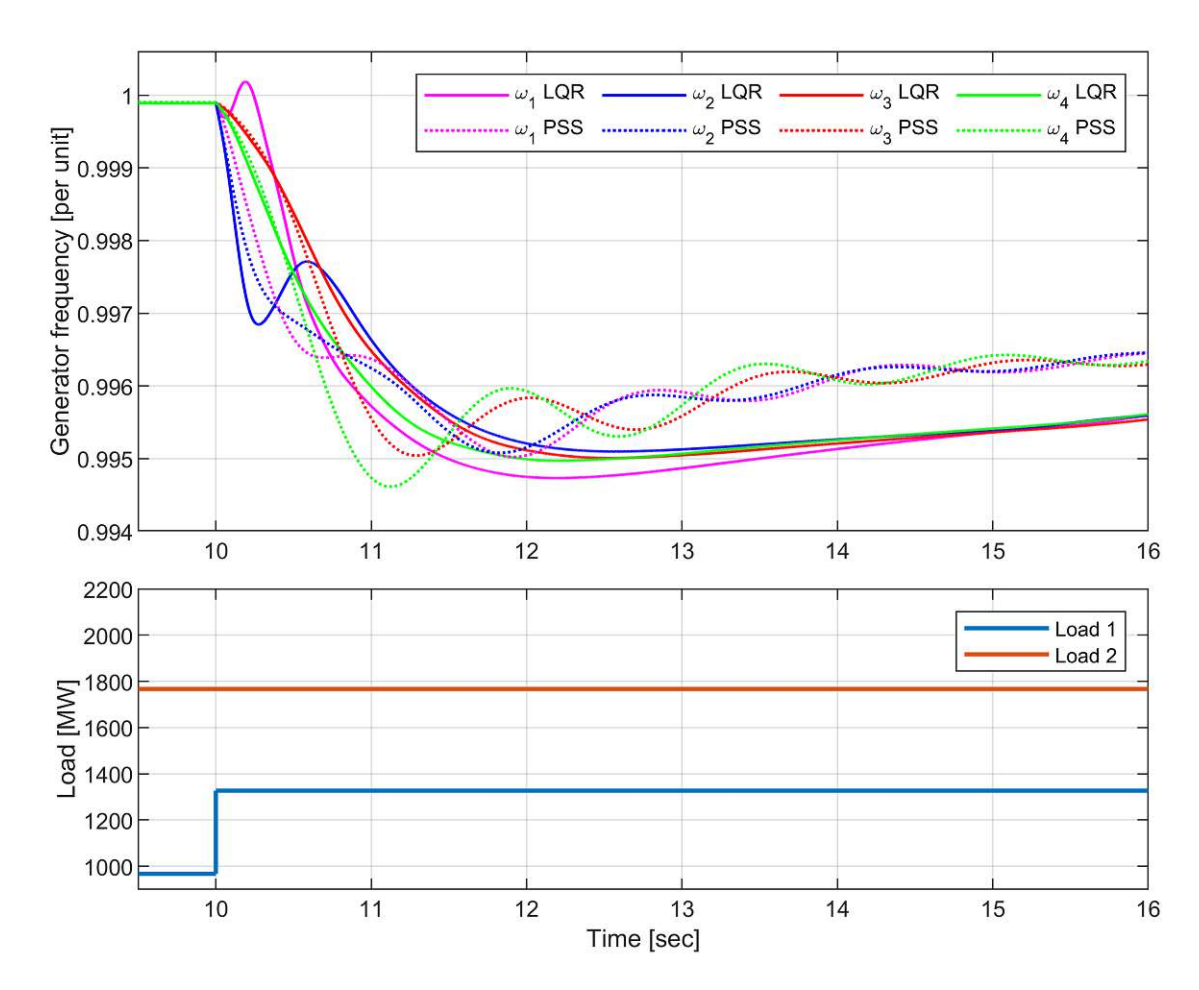


Figure 3.9: Simulink simulation results of a loadstep at Load 1 with the  $\Delta\omega$ feedback LQR controller acting on the stabilization voltage of the generator unit G1.

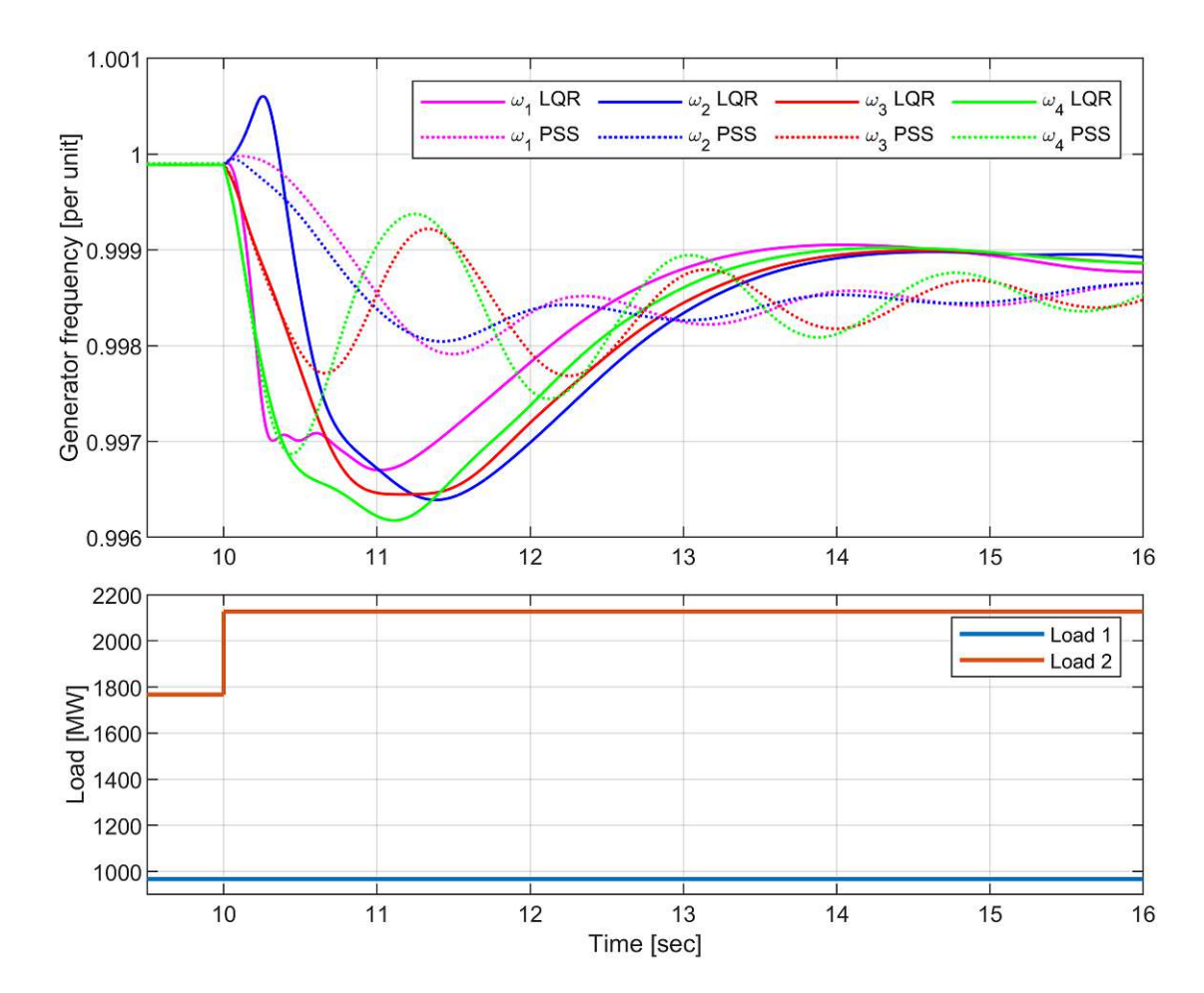


Figure 3.10: Simulink simulation results of a loadstep at Load 2 with the  $\Delta\omega$ feedback LQR controller acting on the stabilization voltage of the generator unit G1.

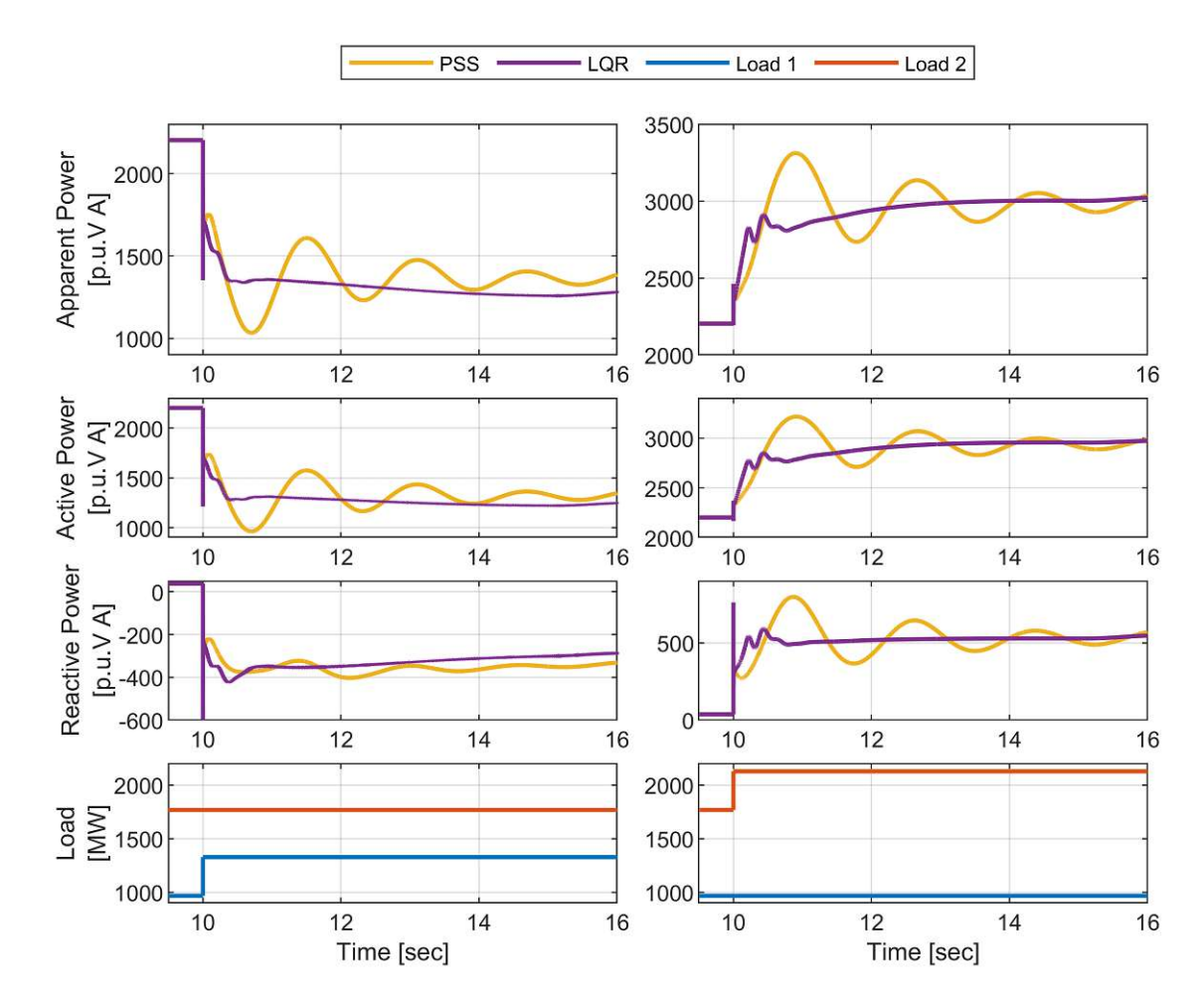


Figure 3.11: Inter-area power transfer from Simulink simulation runs with loadsteps at either Load 1 or Load 2 and the  $\Delta\omega$ -feedback LQR controller installed in generator unit G1.

Model states	full state	Δδ + Δω	Δω
Woder States	feedback	feedback	feedback
G1/SM/Electrical model/φ(1)	0.0042	0	0
G1/SM/Electrical model/φ(2)	0.0220	0	0
G1/SM/Electrical model/φ(3)	0.4735	0	0
G1/SM/Electrical model/φ(4)	0.0055	0	0
G1/SM/Electrical model/φ(5)	0.0287	0	0
G1/SM/Electrical model/φ(6)	0.1052	0	0
G1/SM/Mechanical model/ $\Delta\delta$	-0.2935	-0.1249	0
G1/SM/Electrical model/Negseq. current(1)	2.8589e-12	0	0
G1/SM/Electrical model/Negseq. current(2)	3.8339e-13	0	0
G2/SM/Electrical model/φ(1)	0.0011	0	0
G2/SM/Electrical model/φ(2)	0.0034	0	0
G2/SM/Electrical model/φ(3)	0.0383	0	0
G2/SM/Electrical model/φ(4)	0.0011	0	0
G2/SM/Electrical model/φ(5)	-0.1743	0	0
G2/SM/Electrical model/φ(6)	-0.0934	0	0
G2/SM/Mechanical model/Δδ	-0.5729	-0.3344	0
G2/SM/Electrical model/Negseq. current(1)	7.2819e-13	0	0
G2/SM/Electrical model/Negseq. current(2)	5.7280e-13	0	0
G3/SM/Electrical model/φ(1)	0.0041	0	0
G3/SM/Electrical model/φ(2)	-0.0228	0	0
G3/SM/Electrical model/φ(3)	-0.1491	0	0
G3/SM/Electrical model/φ(4)	-0.0146	0	0
G3/SM/Electrical model/φ(5)	0.3901	0	0
G3/SM/Electrical model/φ(6)	0.1214	0	0
G3/SM/Mechanical model/Δδ	1.0673	0.3461	0
G3/SM/Electrical model/Negseq. current(1)	-2.4311e-12	0	0
G3/SM/Electrical model/Negseq. current(2)	-2.2415e-12	0	0
G4/SM/Electrical model/φ(1)	-0.0117	0	0
G4/SM/Electrical model/φ(2)	-0.0064	0	0
G4/SM/Electrical model/φ(3)	-0.4870	0	0
G4/SM/Electrical model/φ(4)	0.0071	0	0
G4/SM/Electrical model/ф(5)	-0.1832	0	0
G4/SM/Electrical model/ф(6)	-0.1059	0	0
G4/SM/Mechanical model/Δδ	-0.2009	0.1132	0
G4/SM/Electrical model/Negseq. current(1)	-8.5376e-13	0	0
G4/SM/Electrical model/Negseq. current(2)	3.7466e-12	0	0
G1/SM/Mechanical model/Δω	-82.7847	-87.0192	-298.8706
G2/SM/Mechanical model/Δω	-29.7671	-38.4898	-153.5536
G3/SM/Mechanical model/Δω	87.5023	60.0738	209.2502
G4/SM/Mechanical model/Δω	45.3037	62.3510	233.6082

Table 3.2: List of controller gains for the different controller configurations, specified for the corresponding feedback signals, first part.

Model states	full state feedback	Δδ + Δω feedback	Δω feedback
G1/STG/Governor/Speed Regulator/Pos.	0.0732	0	0
G2/STG/Governor/Speed Regulator/Pos.	0.0633	0	0
G3/STG/Governor/Speed Regulator/Pos.	-0.0948	0	0
G4/STG/Governor/Speed Regulator/Pos.	-0.0510	0	0
G2/PSS/Sensor	24.2093	0	0
G2/PSS/Wash-out	-0.8153	0	0
G2/PSS/Lead-lag #1	0.7957	0	0
G2/PSS/Lead-lag #2	-1.4202	0	0
G3/PSS/Sensor	-44.9929	0	0
G3/PSS/Wash-out	1.4839	0	0
G3/PSS/Lead-lag #1	-1.4697	0	0
G3/PSS/Lead-lag #2	2.6232	0	0
G1/EXCITER/Main Regulator	6.2982e-5	0	0
G1/EXCITER/Low Pass Filter 1	-0.2370	0	0
G1/STG/Governor/Speed Regulator/Relay	0.0005	0	0
G2/EXCITER/Main Regulator	5.0462e-6	0	0
G2/EXCITER/Low Pass Filter 1	-0.0163	0	0
G2/STG/Governor/Speed Regulator/Relay	0.0004	0	0
G3/EXCITER/Main Regulator	-1.9319e-5	0	0
G3/EXCITER/Low Pass Filter 1	0.0301	0	0
G3/STG/Governor/Speed Regulator/Relay	-0.0006	0	0
G4/EXCITER/Main Regulator	-6.5291e-5	0	0
G4/EXCITER/Low Pass Filter 1	0.2877	0	0
G4/STG/Governor/Speed Regulator/Relay	-0.0003	0	0
G1/STG/Steam Turbine/Stage 1	0.0602	0	0
G1/STG/Steam Turbine/Stage 2	0.2620	0	0
G1/STG/Steam Turbine/Stage 3	0.2750	0	0
G2/STG/Steam Turbine/Stage 1	0.1469	0	0
G2/STG/Steam Turbine/Stage 2	0.3041	0	0
G2/STG/Steam Turbine/Stage 3	0.3108	0	0
G3/STG/Steam Turbine/Stage 1	-0.1958	0	0
G3/STG/Steam Turbine/Stage 2	-0.4099	0	0
G3/STG/Steam Turbine/Stage 3	-0.4198	0	0
G4/STG/Steam Turbine/Stage 1	-0.0166	0	0
G4/STG/Steam Turbine/Stage 2	-0.1583	0	0
G4/STG/Steam Turbine/Stage 3	-0.1676	0	0

Table 3.3: List of controller gains for the different controller configurations, specified for the corresponding feedback signals, second part.

# 3.3 Stability Analysis

To check that the proposed controller is improving the power grid stability throughout a wide range of operating conditions we apply the proposed controllers on each linearization of the linearization series described in Section 2.1.7. This series consists of 16 linearizations from different operating points of the power grid system within the range of approximately 50% up to 100% of the overall grid capacity rating. We can then analyze the movement of the poles through the controller application for each linearization and gather an approximate idea of the nonlinear system behavior.

This methodology offers a well applicable approach to analyze the stability of a nonlinear system. However, it does not provide a complete stability analysis, since we can not tell what happens in between the snapshots, where we linearize the system. To carry out a complete stability analysis we would have to apply the methodology of analyzing Lyapunov-functions. Although valid Lyapunov-functions do exist for simple generator models, they are very difficult to find for more detailed models [20, 47, 48, 49]. For this reason we stick to the analysis of poles from a linearization series. Figure 3.12 shows the poles of all the 16 different linearized grid models from the aforementioned linearization series without application of a controller. The critical inter-area and inarea-1 and in-area-2 poles of each linearization snapshot show up as tight clusters.

After applying the controller we see that in Figs. 3.13 and 3.14 the influenced poles still show up as distinctive clusters in a more damped location. But, especially in Fig. 3.13, we also see a lot of scattered poles moved into frame from the left in the area  $-(15...7) \pm (10...15)i$ . Those unintentionally moved poles are not yet critical in this configuration, but when tuning the controller more aggressively they might become an issue. However this analysis overall indicates that the proposed controller does not move any pole into an unstable location (right halfplane), but can provide a stability improvement throughout the tested scenario.



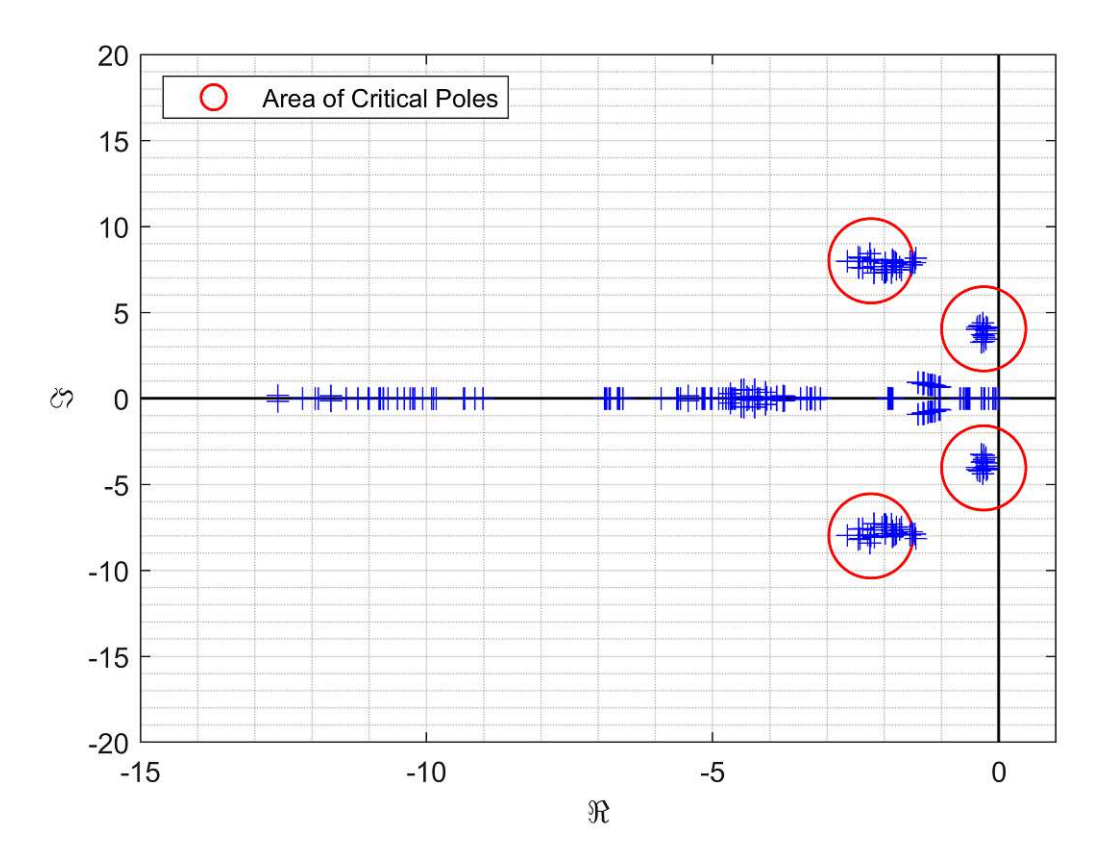


Figure 3.12: Pole locations of the linearized systems throughout the linearization series without the LQR controller at the generator unit G1. The area of the inter-area and in-area-1 poles is additionally marked.

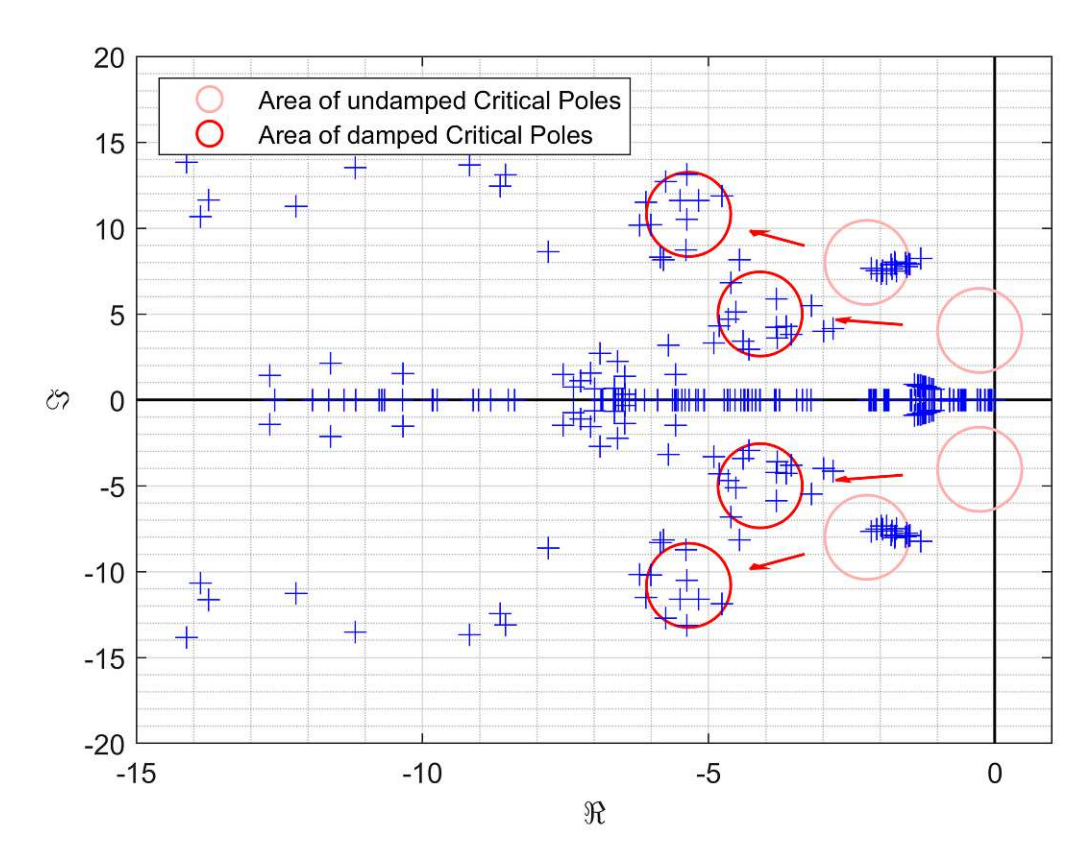


Figure 3.13: Pole locations of the linearized systems throughout the linearization series with the  $\Delta\delta + \Delta\omega$ -feedback LQR controller installed at the generator unit G1. The new area of the inter-area and inarea-1 poles is marked and compared to the initial area location without the LQR controller.

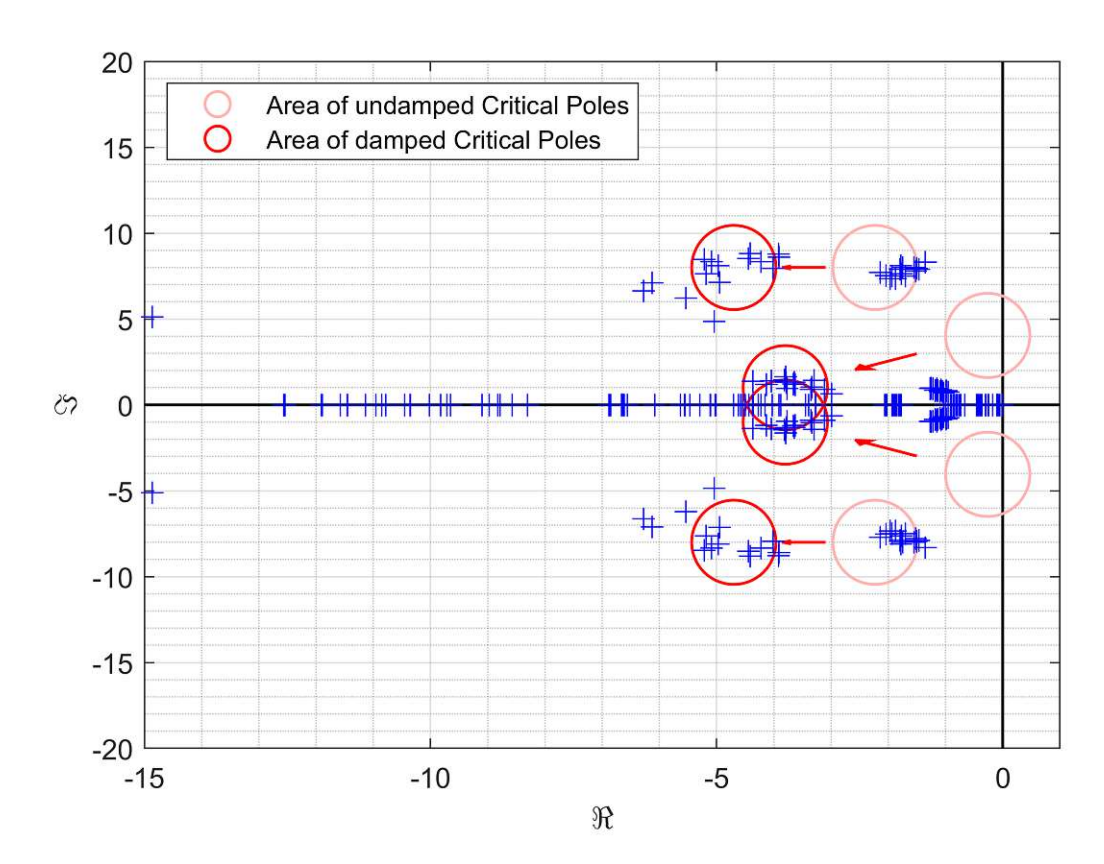


Figure 3.14: Pole locations of the linearized systems throughout the linearization series with the  $\Delta\omega$ -feedback LQR controller installed at the generator unit G1. The new area of the inter-area and in-area-1 poles is marked and compared to the initial area location without the LQR controller.

# Chapter 4

# Conclusion and Outlook

In the scope of this thesis we set up a MATLAB/simulink framework which allows us to get linearization of a high fidelity power grid simulation model, apply linear analysis tools to design controllers and apply and test those controllers on the high fidelity simulation.

We used this simulation framework to design a full state feedback modal damping LQR controller which replaces a conventional PSS device in just one of four generator units in the Kundur-2-Area System. Although the rest of the power grid remains untouched, we show that this modal damping controller is able to effectively dampen generator frequency oscillations after a loadstep scenario. However, the assumption of having an accurate enough feedback of all power grid states in reality is not feasible. Nevertheless those results serve as a valuable benchmark.

Following this benchmark example, we elaborate tools to analytically identify the most important feedback signals for modal observability. Furthermore, we take up a specialized optimization algorithm to design output feedback LQR controllers. These tools allow us in a next step to significantly reduce the number of feedback signals and design modal damping LQR controllers by selecting feedback states via an auxiliary output matrix.

By cleverly selecting only one, respectively two, states per generator unit as feedback signals we are able to extract enough information about the critical oscillation modes to dampen them comparable to the full state feedback. We show that the rotor angle and speed deviations of the four generator units are sufficient feedback signals to design a reduced set modal damping LQR controller.

The generator rotor angle and speed deviations are also chosen with consideration for the introduction of power converter into the power grid. In that case, those states correspond to the phase and frequency deviations of the power converter.

However, implementing power converters into the simulation framework and testing the proposed controllers on the resulting power grid system is still open to future work.

Additionally, the results of this work shall motivate further investigation of the additional grid forming capabilities of power converters. Since they are not restricted by a high physical inertia of a rotor, they might be able to provide an even more effective stabilizing actuation potential.

The results of this work also show useful details for future work of state communication between power plants. As already stated, we can show that the rotor angle and speed deviations are sufficient feedback signals to dampen generator frequency oscillations. Those states are all mechanical states of high inertias and thus behave much slower than electromagnetic states, for example. Hence those states are much less susceptible to communication faults and delays and facilitate their exchange between power plants. In further consequence he presented methods to analyze power grid systems and design damping controllers might also pave the way to reduce the number of feedback signals even more and facilitate damping controllers which rely only on local measurements.

# Appendix A

# Description of state variables

In the following table we use GU as placeholder for the different generator units G1 to G4.

Name	Description
$GU/SM/Electrical\ model/\phi(1)$	Electromagnetic flux component $\phi_q$ ,
	see Eq. (2.3)
$GU/SM/Electrical model/\phi(2)$	Electromagnetic flux component $\phi_d$ ,
	see Eq. (2.3)
$GU/SM/Electrical\ model/\phi(3)$	Electromagnetic flux component $\phi_{fd}$ ,
	see Eq. (2.3)
$GU/SM/Electrical model/\phi(4)$	Electromagnetic flux component $\phi_{kd}$ ,
	see Eq. (2.3)
$GU/SM/Electrical\ model/\phi(5)$	Electromagnetic flux component $\phi_{kq1}$ ,
	see Eq. (2.3)
$\mathrm{GU/SM/Electrical\ model}/\phi(6)$	Electromagnetic flux component $\phi_{kq2}$ ,
	see Eq. (2.3)
${ m GU/SM/Mechanical\ model/}\Delta\delta$	Rotor angle deviation, see Eq. (2.1)
$\mathrm{GU/SM/Mechanical\ model}/\Delta\omega$	Rotor speed deviation, see Eq. (2.1)
GU/SM/Electrical model/	Negative sequence current in d-direction
Negseq. $current(1)$	from usage of symmetric components
GU/SM/Electrical model/	Negative sequence current in q-direction
Negseq. current(2)	from usage of symmetric components
GU/STG/Governor/	Steam valve position, state of
Speed Regulator/Pos.	'Servo-motor position'-block, see Fig. 2.4
GU/STG/Governor/	Steam valve speed, state of
Speed Regulator/Relay	'Speed Relay'-block, see Fig. 2.4



<u>\$</u>
<u>ام</u> ،
Se hut
owled
Sur kn

Name	Description
GU/STG/Steam Turbine/	Mechanical shaft power from the first turbine
Stage 1	stage, state of 'Stage1'-block, see Fig. 2.4
GU/STG/Steam Turbine/	Mechanical shaft power from the second
Stage 2	turbine stage, state of 'Stage2'-block, see
	Fig. 2.4
GU/STG/Steam Turbine/	Mechanical shaft power from the third
Stage 3	turbine stage, state of 'Stage3'-block, see
	Fig. 2.4
GU/EXCITER/Main Regulator	Main regulator for the excitation voltage,
	state of 'Main Regulator'-block, see Fig. 2.5
GU/EXCITER/Low Pass Filter 1	Filter for terminal voltage measurements,
	state of 'Low Pass Filter'-block, see Fig. 2.5
GU/PSS/Sensor	PSS state of 'Sensor'-block, see Fig. 2.6
GU/PSS/Wash-out	PSS state of 'Wash-out'-block, see Fig. 2.6
GU/PSS/Lead-lag #1	PSS state of 'Lead-lag #1'-block, see Fig. 2.6
GU/PSS/Lead-lag #2	PSS state of 'Lead-lag #2'-block, see Fig. 2.6

# TU **Bibliothek**, Die approbierte gedruckte Originalversion dieser Diplomarbeit ist an der TU Wien Bibliothek verfügbar WIEN vour knowledge hub The approved original version of this thesis is available in print at TU Wien Bibliothek.

# Bibliography

- [1] European Commission. Directorate General for Energy. EU energy in figures: statistical pocketbook 2024. Publications Office, LU, 2024.
- [2] Amer Mesanović, Ulrich Münz, and Chris Heyde. Comparison of  $H\infty$ , H2, and pole optimization for power system oscillation damping with remote renewable generation. IFAC-PapersOnLine, 49(27):103–108, January 2016.
- [3] Theodor S. Borsche, Tao Liu, and David J. Hill. Effects of rotational Inertia on power system damping and frequency transients. In 2015 54th IEEE Conference on Decision and Control (CDC), pages 5940–5946, December 2015.
- [4] P. Kundur, J. Paserba, V. Ajjarapu, G. Andersson, A. Bose, C. Canizares, N. Hatziargyriou, D. Hill, A. Stankovic, C. Taylor, T. Van Cutsem, and V. Vittal. Definition and classification of power system stability IEEE/CIGRE joint task force on stability terms and definitions. IEEE Transactions on Power Systems, 19(3):1387–1401, August 2004.
- [5] P. Kundur and Om P. Malik. Power system stability and control. McGraw Hill Education, New York, second edition edition, 2022.
- [6] Amer Mesanović, Ulrich Münz, and Rolf Findeisen. Coordinated tuning of synchronous generator controllers for power oscillation damping. In 2017 IEEE PES Innovative Smart Grid Technologies Conference Europe (ISGT-Europe), pages 1-6, September 2017.
- [7] Bahram Shakerighadi, Nicklas Johansson, Robert Eriksson, Pinaki Mitra, Alberto Bolzoni, Angel Clark, and Hans-Peter Nee. An overview of stability challenges for power-electronic-dominated power systems: The grid-forming approach. IET Generation, Transmission & Distribution, 17(2):284–306, January 2023.
- [8] Toshinobu Shintai, Yushi Miura, and Toshifumi Ise. Oscillation Damping of a Distributed Generator Using a Virtual Synchronous Generator. IEEE Transactions on Power Delivery, 29(2):668–676, April 2014.

[9] Huijie Cheng, Zhikang Shuai, Chao Shen, Xuan Liu, Zuyi Li, and Z. John Shen. Transient Angle Stability of Paralleled Synchronous and Virtual Synchronous Generators in Islanded Microgrids. IEEE Transactions on Power Electronics, 35(8):8751–8765, August 2020.

- [10] U.P. Mhaskar and A.M. Kulkarni. Power oscillation damping using FACTS devices: modal controllability, observability in local signals, and location of transfer function zeros. IEEE Transactions on Power Systems, 21(1):285–294, February 2006.
- [11] Xiaoqing Yang and A. Feliachi. Stabilization of inter-area oscillation modes through excitation systems. IEEE Transactions on Power Systems, 9(1):494–502, February 1994.
- [12] M.E. Aboul-Ela, A.A. Sallam, J.D. McCalley, and A.A. Fouad. Damping controller design for power system oscillations using global signals. IEEE Transactions on Power Systems, 11(2):767–773, May 1996.
- [13] M. Noroozian and G. Adersson. Damping of power system oscillations by use of controllable components. IEEE Transactions on Power Delivery, 9(4):2046–2054, October 1994.
- [14] Abhineet Prakash, Mohamed Shawky El Moursi, S. K. Parida, and Ehab F. El-Saadany. Design of Adaptive Damping Controller With Wide-Area Measurements Considering Unknown Power System Dynamics. IEEE Transactions on Power Systems, 39(3):5150–5162, May 2024.
- [15] Mohamed Ramadan Younis and Reza Iravani. Wide-area damping control for inter-area oscillations: A comprehensive review. In 2013 IEEE Electrical Power &Energy Conference, pages 1–6, August 2013.
- [16] Robin Preece, Jovica V. Milanovic, Abddulaziz M. Almutairi, and Ognjen Mar-Damping of inter-area oscillations in mixed AC/DC networks using WAMS based supplementary controller. *IEEE Transactions on Power Systems*, 28(2):1160–1169, May 2013.
- [17] M. Ehsan Raoufat, Kevin Tomsovic, and Seddik M. Djouadi. Virtual Actuators for Wide-Area Damping Control of Power Systems. IEEE Transactions on Power Systems, 31(6):4703–4711, November 2016.
- [18] MathWorks, Inc. Kundur's Two-Area System with PMU; This example shows the use of the PMU (PLL-Based, Positive-Sequence) block within the Kundur's Two-Area System. https://de.mathworks.com/help/sps/ug/



- pmu-pll-based-positive-sequence-kundur-s-two-area-system.html, 2025. Accessed: 2025-03-06.
- [19] MathWorks, Inc. Synchronous Machine pu Standard; Model dynamics of three-phase round-rotor or salient-pole synchronous machine using standard parameters in pu units. https://de.mathworks.com/help/sps/powersys/ref/synchronousmachinepustandard.html, 2025. Accessed: 2025-03-02.
- [20] IEEE Guide for Synchronous Generator Modeling Practices and Parameter Verification with Applications in Power System Stability Analyses. *IEEE Std 1110-2019* (Revision of IEEE Std 1110-2002), pages 1–92, March 2020.
- [21] Florian Dorfler and Francesco Bullo. Kron Reduction of Graphs With Applications to Electrical Networks. *IEEE Transactions on Circuits and Systems I: Regular Papers*, 60(1):150–163, January 2013.
- [22] M. Pondini, A. Signorini, V. Colla, and S. Barsali. Analysis of a simplified Steam Turbine governor model for power system stability studies. *Energy Procedia*, 158:2928–2933, February 2019.
- [23] IEEE Committee Report. Dynamic Models for Steam and Hydro Turbines in Power System Studies. *IEEE Transactions on Power Apparatus and Systems*, PAS-92(6):1904–1915, November 1973.
- [24] MathWorks, Three-Phase Transformer (Two Windings); Inc. Implement three-phase transformer with configurable winding connections. https://de.mathworks.com/help/sps/powersys/ref/ threephasetransformertwowindings.html, 2025. Accessed: 2025-02-28.
- [25] MathWorks, Inc. Three-Phase PI Section Line; Implement three-phase transmission line section with lumped parameters. https://de.mathworks.com/help/sps/powersys/ref/threephasepisectionline.html, 2025. Accessed: 2025-02-28.
- [26] MathWorks, Inc. Specialized Power Systems; Model electrical power systems using specialized components and algorithms. https://de.mathworks.com/help/sps/specialized-power-systems.html, 2025. Accessed: 2025-02-28.
- [27] MathWorks, Inc. Introducing the Phasor Simulation Method. https://de.mathworks.com/help/sps/powersys/ug/introducing-the-phasor-simulation-method.html, 2025. Accessed: 2025-02-28.



[28] MathWorks, Inc. Model Linearizer; Linearize Simulink models. de.mathworks.com/help/slcontrol/ug/modellinearizer-app.html, 2025. Accessed: 2025-02-28.

- [29] I. J. Perez-arriaga, G. C. Verghese, and F. C. Schweppe. Selective Modal Analysis with Applications to Electric Power Systems, PART I: Heuristic Introduction. IEEE Transactions on Power Apparatus and Systems, PAS-101(9):3117-3125, September 1982.
- [30] Steven H. Weintraub. Jordan Canonical Form: Theory and Practice. Morgan & Claypool Publishers, 2009. Google-Books-ID: qDPMLisVSCIC.
- [31] Steven H. Weintraub. Jordan Canonical Form: Application to Differential Equations. Morgan & Claypool Publishers, September 2008. Google-Books-ID: mYZi-AQAAQBAJ.
- [32] Qian Tang, Fuyu Guo, Tao Huang, Kaiming Yang, Yu Zhu, and Min Li. Modal-Decomposition-Dependent State-Space Modeling and Modal Analysis of a Rigid-Flexible, Coupled, Multifreedom Motion System: Theory and Experiment. Shock and Vibration, 2020:1–16, August 2020.
- [33] Vasile-Mihai Popov. Hyperstability of Control Systems. Springer Berlin Heidelberg, Berlin, Heidelberg, 1973.
- [34] Vitold Belevitch. Classical network theory., 1968.
- [35] H. M. A. Hamdan and A. M. A. Hamdan. On the coupling measures between modes and state variables and subsynchronous resonance. Electric Power Systems Research, 13(3):165–171, December 1987.
- [36] A. M. A. Hamdan and A. M. Jaradat. Modal Controllability and Observability of Linear Models of Power Systems Revisited. Arabian Journal for Science and Engineering, 39(2):1061–1066, February 2014.
- [37] Linash P. Kunjumuhammed and Bikash C. Pal. Selection of Feedback Signals for Controlling Dynamics in Future Power Transmission Networks. IEEE Transactions on Smart Grid, 6(3):1493–1501, May 2015.
- [38] A. Heniche and I. Karnwa. Control loops selection to damp inter-area oscillations of electrical networks. IEEE Transactions on Power Systems, 17(2):378–384, May 2002.



[39] G. C. Verghese, I. J. Perez-arriaga, and F. C. Schweppe. Selective Modal Analysis With Applications to Electric Power Systems, Part II: The Dynamic Stability Problem. IEEE Transactions on Power Apparatus and Systems, PAS-101(9):3126-3134, September 1982.

- [40] G. C. Verghese, I. J. Pérez-Arriaga, and F. C. Schweppe. Measuring State Variable Participation for Selective Modal Analysis 1. IFAC Proceedings Volumes, 15(1):501– 505, January 1982.
- [41] MathWorks, Inc. lqr(); Design of a linear quadratic regulator (LQR). https: //de.mathworks.com/help/control/ref/lti.lqr.html, 2025. Accessed: 2025-02-28.
- [42] Hametner C. and Jakubek S. Zustandrsregelung von Mehrgrößensystemen. Lecture script, 2023.
- [43] Frank L. Lewis, Draguna L. Vrabie, and Vassilis L. Syrmos. Optimal Control. Wiley, 1 edition, January 2012.
- [44] Adrian Ilka and Nikolce Murgovski. Novel Results on Output-Feedback LQR Design. IEEE Transactions on Automatic Control, 68(9):5187–5200, September 2023.
- [45] Adrian Ilka. Matlab/Octave toolbox for structurable and robust output-feedback LQR design\*. IFAC-PapersOnLine, 51(4):598-603, January 2018.
- [46] Adrian Ilka, Nikolce Murgovski, and Jonas Sjöberg. An iterative Newton's method for output-feedback LQR design for large-scale systems with guaranteed convergence. In 2019 18th European Control Conference (ECC), pages 4849–4854, June 2019.
- [47] R.J. Davy and I.A. Hiskens. Lyapunov functions for multimachine power systems with dynamic loads. IEEE Transactions on Circuits and Systems I: Fundamental Theory and Applications, 44(9):796–812, September 1997.
- [48] Marian Anghel, Federico Milano, and Antonis Papachristodoulou. Algorithmic Construction of Lyapunov Functions for Power System Stability Analysis. IEEE Transactions on Circuits and Systems I: Regular Papers, 60(9):2533–2546, September 2013.
- [49] M. A. Mahmud, M. J. Hossain, H. R. Pota, and M. S. Ali. Generalized Lyapunov function for stability analysis of interconnected power systems. In AUPEC 2011, pages 1–6, September 2011.

